RESTRICTED

Copy No. 8

RM No. A8E12

NACA RM No. A8E12

SEP 22 1947

3193
53
c.1

NACA
CLASSIFICATION CANCELLED
By new form 243, 7-3-50

RESEARCH MEMORANDUM

EFFECT OF A NACELLE ON THE LOW-SPEED AERODYNAMIC CHARACTERISTICS OF A SWEPT-BACK WING

By Frederick H. Hanson, Jr. and Robert E. Dannenberg

Ames Aeronautical Laboratory,
Moffett Field, Calif.

CLASSIFIED DOCUMENT

This document contains classified information affecting the National Defense of the United States within the meaning of the Espionage Act, USC 50:31 and 32. Its transmission or the revelation of its contents in any manner to an unauthorized person is prohibited by law. Information so classified may be imparted only to persons in the military and naval services of the United States, appropriate civilian officers and employees of the Federal Government who have a legitimate interest therein, and to United States citizens of known loyalty and discretion who of necessity must be informed thereof.

NATIONAL ADVISORY COMMITTEE FOR AERONAUTICS

WASHINGTON
July 21, 1948

RESTRICTED

N A C A LIBRARY
LANGLEY MEMORIAL AERONAUTICAL LABORATORY
Langley Field, Va.

NASA Technical Library
3 1176 01434 4577

NATIONAL ADVISORY COMMITTEE FOR AERONAUTICS

RESEARCH MEMORANDUM

EFFECT OF A NACELLE ON THE LOW-SPEED AERODYNAMIC CHARACTERISTICS OF A SWEPT-BACK WING

By Frederick H. Hanson, Jr. and Robert E. Dannenberg

SUMMARY

Wind-tunnel tests of a simplified nacelle on a semispan wing having approximately 35° of sweepback were made to determine the effects of the nacelle on the aerodynamic characteristics of the wing. The wing-nacelle combination was tested with the nacelle mounted in several positions on the wing and on a strut below the wing. The wing had an aspect ratio of 6.04 and a ratio of tip chord to root chord of 0.5.

The experimental results indicate that the nacelle had only small effects on the lift and pitching-moment characteristics of the wing. Pressure-distribution measurements for a high-speed attitude of the various wing-mounted nacelles showed that the local velocities near the nacelle were less than the maximum velocities over the wing alone, except for the nacelle extending forward from the leading edge of the wing. With the nacelle attached to the wing by a strut, the local juncture velocities were considerably in excess of the maximum wing velocities.

INTRODUCTION

The design of a satisfactory wing-nacelle combination becomes more critical as operating speeds approach the velocity of sound. The application of swept wings to delay adverse compressibility effects to higher speeds has particularly intensified the problems of the nacelle designer.

A nacelle mounted on a swept wing should not adversely affect the high-speed characteristics of the wing or aggravate its low-speed characteristics. If the local velocities and pressure

gradients for a swept-wing-nacelle combination are as low as those of the wing without the nacelle, the advantages of the swept wing at transonic speeds may be preserved. A nacelle should not produce an undue increase in drag or change of the span loading. The longitudinal instability, evident near the stall for certain swept wings, should not be aggravated by a nacelle; in fact, alleviation of this condition without changing the stability at lower lift coefficients would be desirable.

An experimental investigation has been undertaken in the Ames 7- by 10-foot wind tunnel to evaluate the effects of a nacelle on the characteristics of a swept wing at low and moderate speeds and to provide information to be used as a guide for the study of nacelles on swept wings at high speeds. This report presents the experimental results obtained with a simplified nacelle mounted in several positions on a wing having approximately 35° of sweepback. The nacelle was simulated by an ellipsoid having a fineness ratio of 5.0 and did not incorporate internal air flow.

COEFFICIENTS, SYMBOLS, AND CORRECTIONS

The following standard NACA coefficients and symbols are used:

C_L lift coefficient $\left(\frac{L}{q_oS}\right)$

C_D drag coefficient $\left(\frac{D}{q_oS}\right)$

C_{D_F} drag coefficient of nacelle based on frontal area of nacelle $\left(\frac{\Delta D}{q_oF}\right)$

C_m pitching-moment coefficient $\left(\frac{M}{q_oS\bar{c}}\right)$

α angle of attack, degrees

α_u uncorrected angle of attack, degrees

P pressure coefficient $\left(\frac{p - p_o}{q_o}\right)$

L lift, pounds

D drag, pounds

ΔD drag increment due to nacelle, pounds

M pitching-moment about a lateral axis through the one-quarter-chord point of the mean aerodynamic chord, foot-pounds

S wing area, square feet

F frontal area of nacelle, square feet

$\bar{c}$ mean aerodynamic chord, feet

q_o free-stream dynamic pressure, pounds per square foot

p local static pressure, pounds per square foot

p_o free-stream static pressure, pounds per square foot

b span of complete wing, feet

c_n chord of wing at 0.31 b/2, feet

The test results presented have been corrected for fluid compressibility. Jet-boundary corrections were obtained by the method developed in reference 1 modified for consideration of the sweepback. The jet-boundary corrections added to the angles of attack and drag coefficients were 0.985 C_L and 0.020 C_L^2, respectively. The effects of the boundary layer above the dummy floor and of air leakage between the wing root and the floor plates on the characteristics of the model were not determined. These effects were presumably small and probably did not influence the effects of the nacelle on the wing characteristics.

MODEL AND APPARATUS

The model wing of 5-foot semispan used for these tests had an NACA 64_1-212 airfoil section (section taken perpendicular to the 27.06-percent wing-chord line), a ratio of tip chord to root chord of 0.5, and an aspect ratio of 6.04. A sketch of the plan form of the wing is shown in figure 1. The 27.06-percent chord line of the wing was swept back 35°. No twist was incorporated in the wing. Coordinates for the NACA 64_1-212 airfoil section are presented in table I. Coordinates for sections parallel to the direction of free-stream air flow are presented in table II. The wing tip is shown in figure 2.

The nacelle was a prolate ellipsoid of revolution having major and minor axes of 30 inches and 6 inches, respectively, corresponding

to 1.331 and 0.266 of the wing chord at the spanwise location of the nacelle. This ellipsoid was mounted at 31 percent of the wing semispan with its major axis parallel to the chord plane of the wing and the simulated plane of symmetry. Figure 3 shows the eight positions in which the nacelle was mounted on the wing or attached to the wing by a strut. The nacelle positions are tabulated in table III. The mounting strut had an NACA 65-009 airfoil section with a chord of 10 inches.

The semispan wing was mounted so that a dummy tunnel floor served as a reflection plane simulating a plane of symmetry. The dummy floor separated the boundary layer of the tunnel floor from the model and extended 8 feet upstream and 9 feet downstream from the center of rotation of the model. A fairing was provided around the portion of the model between the turntables of the dummy floor and the tunnel floor. A gap of approximately one-eighth inch between the end of the model and the turntable of the dummy floor was necessary to allow the forces acting on the model to be measured by the normal wind-tunnel balance system. This gap was made small to keep air leakage into the tunnel near the model to a minimum.

The pressure distributions over the model were measured by flush orifices that were connected to multiple-tube manometers. The locations of the rows of static-pressure orifices on the model are shown in figures 1 and 3.

RESULTS AND DISCUSSION

The test results are presented for a Mach number of 0.24 and a Reynolds number of 2,700,000 based upon the wing mean aerodynamic chord.

Force and Moment Characteristics

The aerodynamic characteristics of the wing and the various wing-nacelle combinations are shown in figure 4. In general, these data indicate that the nacelle in its various positions had only small effects on the lift of the wing. The effects of the nacelle in various positions on the angle of attack for zero lift are summarized in table III. The largest increase in the angle of attack for zero lift was 0.6° and occurred with the nacelle underslung and projecting well forward of the wing leading edge (fig. 4(d)). In this same position the nacelle also slightly reduced the slope of the lift curve near maximum lift. The slope of the lift curve remained

relatively unaffected with the nacelle in the other positions. The effect of the nacelle on the maximum lift coefficient was less than 0.02 for all positions tested.

Drag-coefficient increments attributable to the addition of the nacelle have been evaluated from the data of figure 4 and are presented in figure 5 as nacelle drag coefficients (based on the frontal area of the nacelle). The drag coefficients of the nacelle mounted in various positions on the strut (based on the frontal area of the strut and nacelle) were, to all practical purposes, equal and are represented by a single curve in figure 5. The data show that, with the trailing edge of the nacelle terminating on the wing, an abrupt increase in drag coefficient occurred at lower lift coefficients than with the trailing edge of the nacelle behind the wing. This abrupt increase of drag coefficient was probably due to separation of flow from the junctures of the nacelle and wing. The nacelle in an underslung position had a considerably higher minimum drag than in the other locations. Acute surface intersections are evident for the underslung position in figure 3(a), and it is believed the large difference in minimum drag was due to separation occurring at the juncture of the trailing edge of the underslung nacelle and the wing. The drag of the nacelle in the underslung position could probably have been reduced with a proper trailing-edge fairing or by extending the nacelle behind the trailing edge of the wing.

The variation of the drag coefficient with Reynolds number for the wing and for the wing with the nacelle in the central position with its leading edge at 40 percent of the wing chord is presented in figure 6. It is noted that the drag increment due to the nacelle remained relatively constant throughout the Reynolds number range investigated. The variations of drag increment with Reynolds number for the nacelle in the other positions, either on the wing or strut, were also relatively constant and are not presented.

The nacelle was slightly destabilizing in the two positions well forward on the wing, as indicated by the variation of pitching-moment coefficient with lift coefficient in figure 4. Increments of dC_m/dC_L attributable to the nacelle have been measured from figure 4 near zero lift and are presented in table III. As the nacelle was moved aft, the destabilizing effect near zero lift was reduced, with the nacelle centrally mounted. In the two aft locations, the centrall mounted nacelle improved the stability for lift coefficients just below the stall. For angles of attack above the stall, the wing and all combinations of the wing and nacelle were unstable.

Wing Pressure Distribution

As little information was available on the pressure distribution over swept-back wings, pressure studies of the wing were made at 15, 31, 55, 73.3, and 91.7 percent of the semispan and are presented in figure 7. The spanwise pressure distribution at 40 percent of the wing chord is shown in figure 8. Simple sweepback considerations indicate that pressure coefficients for a swept wing should vary as the square of the cosine of the angle of sweep. For the wing used in these tests, the stagnation pressure coefficient should then be 0.63 instead of 1.0 as in the case of an unswept wing. This value is in close agreement with the test results obtained at zero angle of attack. Near the wing tip, the measured stagnation pressure coefficient became larger than the calculated value, presumably due to the change in flow conditions around the wing tip.

In order to determine the effect of restriction of the spanwise flow on the pressure coefficients of the swept wing, a 3-foot-diameter flat plate was mounted at 31 percent of the semispan and parallel to the plane of symmetry as shown in figure 9. It may be seen in figure 10 that this restriction of the spanwise flow increased the velocities over the forward portion of the wing and decreased the general level of velocities over the aft portion of the wing. In figure 11(a) are shown contours of constant pressure coefficients (data obtained from orifices in the plate) in the region of the wing leading edge on the inboard side of the flat plate. It is indicated in figure 11(a) that a region of high velocity might be expected at the inboard leading-edge juncture of a swept-back wing and nacelle, if the nacelle extends forward of the wing.

Wing-Nacelle Pressure Distribution

The pressure distributions over the upper- and lower-surface center lines of the nacelle in the various positions on the wing are presented in figure 12. The lowest velocities along these center lines were obtained with the nacelle in the farthest aft position, that is, with the leading edge of the nacelle at 40 percent of the wing chord. The nacelle in any of the positions on the wing had maximum velocities along its upper- and lower-surface center lines which were less than the maximum velocities over the wing without the nacelle.

The pressure distribution over the wing-nacelle junctures for the nacelle in the various positions on the wing are presented in figures 13 to 16. These data indicate that, with the leading edge

of the nacelle at or behind the leading edge of the wing (figs. 14 and 15), the velocities occurring in the junctures of the wing and nacelle were less than the maximum velocities over the wing alone for high-speed angles of attack ($\alpha_u = 0^\circ$ to 2°). With the nacelle extended forward from the wing leading edge (figs. 13 and 16), the local velocities in the forward portion of the inboard juncture were considerably in excess of the maximum velocities over the wing alone. For the nacelle in a central position well forward on the wing, this excess velocity region was greatest on the upper surface and extended back to about 30 percent of the wing chord for angles of attack between 0° and 2°. For the nacelle in an underslung position at an angle of attack of 0° the inboard lower juncture had an excess velocity region that extended back to approximately 50 percent of the wing chord. At an angle of attack of 2°, however, the inboard lower juncture for the underslung position of the nacelle was satisfactory, and the only excess velocities evident were in a highly localized region near the leading edge of the inboard upper juncture.

In order to compare the juncture pressures with those indicated by the flat-plate tests, the nacelle in a central position well forward on the wing was equipped with sufficient pressure orifices to permit determination of the inboard surface pressure distribution. A comparison of the pressures over the nacelle and the flat plate is given in figure 11. The difference between the two pressure-contour diagrams at low angles of attack is small. At 4° and 6° angle of attack, however, the pressures on the plate were less than those over the nacelle, indicating that the three-dimensional nacelle did not block the spanwise flow as completely as did the flat plate.

The pressure distribution over the wing and nacelle was measured for four positions of the nacelle on a strut beneath the wing. Two strut lengths were used in conjunction with two fore-and-aft locations of the nacelle on the strut. Figure 17 presents the effect of strut length on the pressures along the inboard and outboard wing-strut juncture with the nacelle extended 40 percent of the wing chord forward of the wing leading edge. Figure 18 is similar to figure 17 except that the pressures were measured along the wing-strut juncture with the nacelle leading edge directly below the wing leading edge. In all cases, the pressures in the wing-strut juncture for high-speed angles of attack indicated velocities in excess of those over the plain wing. The highest velocities occurred along the inboard side of the short strut with the nacelle mounted in the forward position. The smallest velocities in the wing-strut juncture were obtained with the longer strut and with the nacelle mounted in the coincident position.

In figure 19 are presented the pressure distributions in the juncture between the nacelle and the strut. For an angle of attack of 0°, the pressures in the nacelle-strut juncture indicated that velocities greater than those over the wing alone were present. For an angle of attack of 2°, the velocities indicated for the nacelle-strut juncture were less than those over the wing alone except for the inboard juncture with the nacelle forward on the strut. The smallest velocities along the nacelle-strut juncture were obtained with the longer strut and the nacelle mounted in the coincident position.

Although high local velocities occurred in the wing-strut and nacelle-strut junctures investigated, it is believed that considerably lower local velocities could be obtained by proper location of the strut with respect to the wing and nacelle. The location of the strut on the wing was particularly undesirable since the positions of the minimum pressures for the wing and strut were nearly coincident.

The effect of the nacelle on the spanwise pressure distribution at 40 percent of the wing chord is presented in figure 20. These data are not indicative of the minimum pressures provided by the nacelle in the various positions, but do serve to indicate the effects of the nacelle on the spanwise pressure distribution. It should be noted that the higher velocities occurring on the wing lower surface with the nacelle in any of the underslung positions produced a loss of lift for these sections. This would increase the wing-root bending moments and the induced drag for an airplane at a given lift condition. Evident from figure 20(b) are the previously mentioned high velocities occurring in the wing-strut juncture.

Air Flow Over the Swept-Back Wing

Tuft studies made on the plain wing indicated that the direction of air flow at low angles of attack was slightly outboard over approximately the forward 7 percent of the wing chord. Between 7 percent and about 50 percent of the wing chord the air flow was directed slightly inboard, and from 50 percent of the wing chord to the trailing edge the air flow had a small outboard component. As the angle of attack of the wing was increased, the tufts near the trailing edge were directed more toward the tip, indicating more spanwise flow. Tufts 0.25 inch above the wing surface and supported by wires from and normal to the surface indicated considerably less spanwise flow than did those directly on the wing surface.

Figure 21 shows the direction of air flow with reference to the free-stream direction at 31 percent of the wing semispan and 0.25 inch from the upper and lower surfaces of the wing for an angle of attack of 0°. These data were obtained by means of the small prong-type directional pitot also shown in figure 21. The data indicate the same general type of streamline pattern as the tuft studies except near the trailing edge of the wing where the tufts on the wing surface showed a flow toward the tip.

Tuft studies made with the nacelle projecting forward from the wing in central and underslung positions showed that localized separation of the air first occurred at the inboard juncture near the wing leading edge at an angle of attack between 6° and 8°. (See fig. 22(a) and (b).) With the nacelle leading edge coincident with or aft of the wing leading edge, however, separation appeared first in the outboard junctures after an angle of attack of 14° had been exceeded. (See fig. 22(c) and (d).)

CONCLUDING REMARKS

The results of this low-speed experimental investigation indicate that the addition of the nacelle to the 35° swept-back wing had only small effects on the lift and pitching-moment characteristics of the wing alone. The differences in the force and moment characteristics of the wing-nacelle combinations for the various positions of the nacelle were also found to be small.

Pressure-distribution studies of the wing and nacelle for attitudes corresponding to high-speed flight indicate several interesting characteristics. The velocities over the upper- and lower-surface center lines of the nacelle were less than the maximum velocities over the wing without the nacelle. With the nacelle extended forward from the leading edge of the wing, the local velocities in the forward portion of the inboard juncture were considerably in excess of the maximum velocities over the wing alone. With the leading edge of the nacelle at or behind the leading edge of the wing, the velocities occurring in the junctures of the wing and nacelle were less than the maximum velocities over the wing alone. With the nacelle attached to the wing by a strut, velocities considerably in excess of those over the wing alone were found in the wing-strut juncture for the single position of the strut tested. The velocities occurring in the nacelle-strut junctures were somewhat lower than those in the wing-strut junctures; however, they were

TABLE II

COORDINATES FOR SECTIONS
PARALLEL TO FREE AIR STREAM

[Stations and ordinates given in percent of airfoil chord]

Upper surface		Lower surface	
Station	Ordinate	Station	Ordinate
0	0	0	0
.465	.908	.647	-.820
.733	1.103	.935	-.979
1.275	1.411	1.504	-1.221
2.644	1.961	2.905	-1.632
5.388	2.754	5.679	-2.196
8.129	3.355	8.426	-2.608
10.859	3.846	11.153	-2.939
16.279	4.614	16.555	-3.439
21.647	5.175	21.890	-3.794
26.959	5.580	27.163	-4.035
32.213	5.845	32.378	-4.177
37.413	5.978	37.534	-4.220
42.555	5.983	42.635	-4.165
47.644	5.816	47.680	-3.968
52.674	5.525	52.674	-3.673
57.649	5.135	57.618	-3.307
62.569	4.666	62.512	-2.887
67.433	4.133	67.358	-2.432
72.242	3.551	72.156	-1.954
76.998	2.934	76.909	-1.471
81.701	2.297	81.616	-1.003
86.350	1.662	86.279	-.573
90.948	1.049	90.899	-.216
95.497	.484	95.473	.022
100.000	0	100.000	0

NACA

TABLE III

EFFECT OF THE NACELLE ON ANGLE OF ATTACK FOR ZERO LIFT AND LONGITUDINAL STABILITY OF THE WING

Nominal position	Nacelle position		Increase in angle of zero lift due to nacelle (deg)	Increase in $\frac{dC_m}{dC_L}$ near zero lift due to nacelle
	Vertical position of nacelle center line with reference to wing-chord plane	Longitudinal position of nacelle leading edge with reference to wing leading edge		
Central-forward	Coincident	Forward 40-percent c_n	0.1	0.02
Central-coincident	Coincident	Coincident	.2	0
Central-aft	Coincident	Aft 40-percent c_n	.2	0
Underslung-forward	Underslung 7.3-percent c_n	Forward 40-percent c_n	.6	.02
Underslung-forward on 4-inch strut	Underslung 33.1-percent c_n	Forward 40-percent c_n	.3	.01
Underslung-forward on 6-inch strut	Underslung 42.0-percent c_n	Forward 40-percent c_n	.4	0
Underslung-coincident on 4-inch strut	Underslung 33.1-percent c_n	Coincident	0	.01
Underslung-coincident on 6-inch strut	Underslung 42.0-percent c_n	Coincident	0	.01

WING AREA = 8.283 SQ. FT. (SEMISPAN)
ASPECT RATIO = 6.04 (BASED ON FULL SPAN)
M.A.C. = 1.728 FT. (PARALLEL TO ROOT CHORD)
TAPER RATIO = 0.5
AIRFOIL SECTION NACA 64_1-212
(PERPENDICULAR TO THE 27.06-PERCENT WING CHORD LINE)

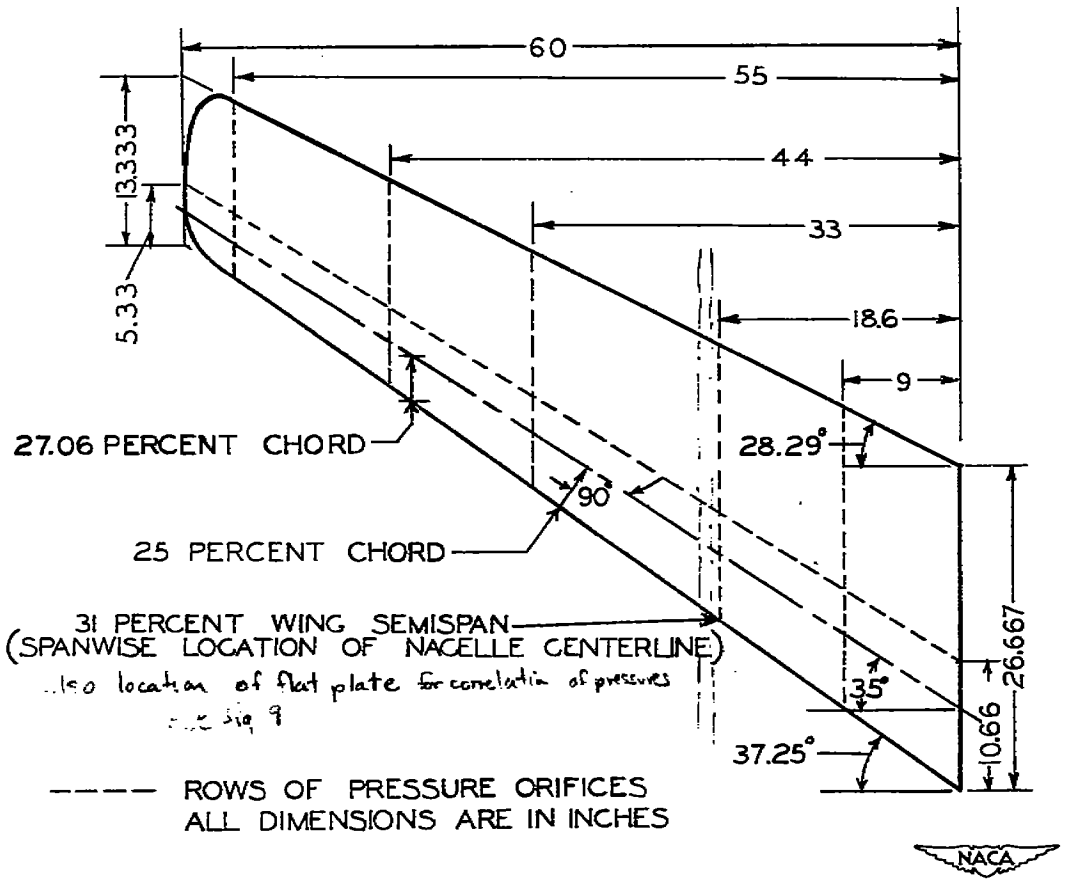

FIGURE 1.— PLAN FORM OF MODEL WING.

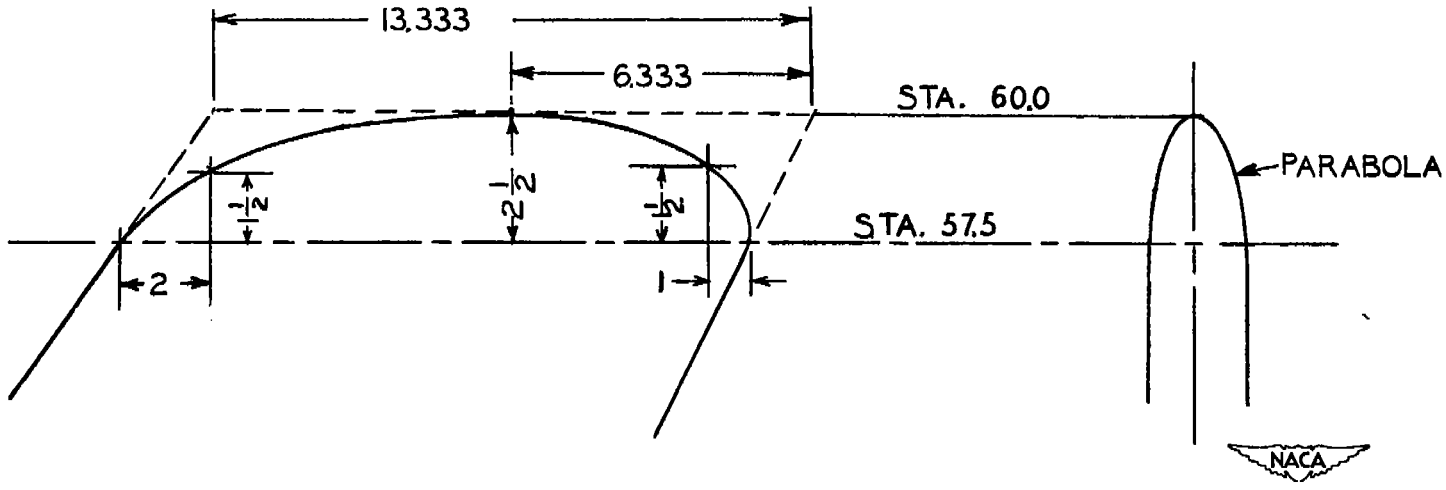

ALL DIMENSIONS ARE IN INCHES

FIGURE 2.- WING TIP SHAPE

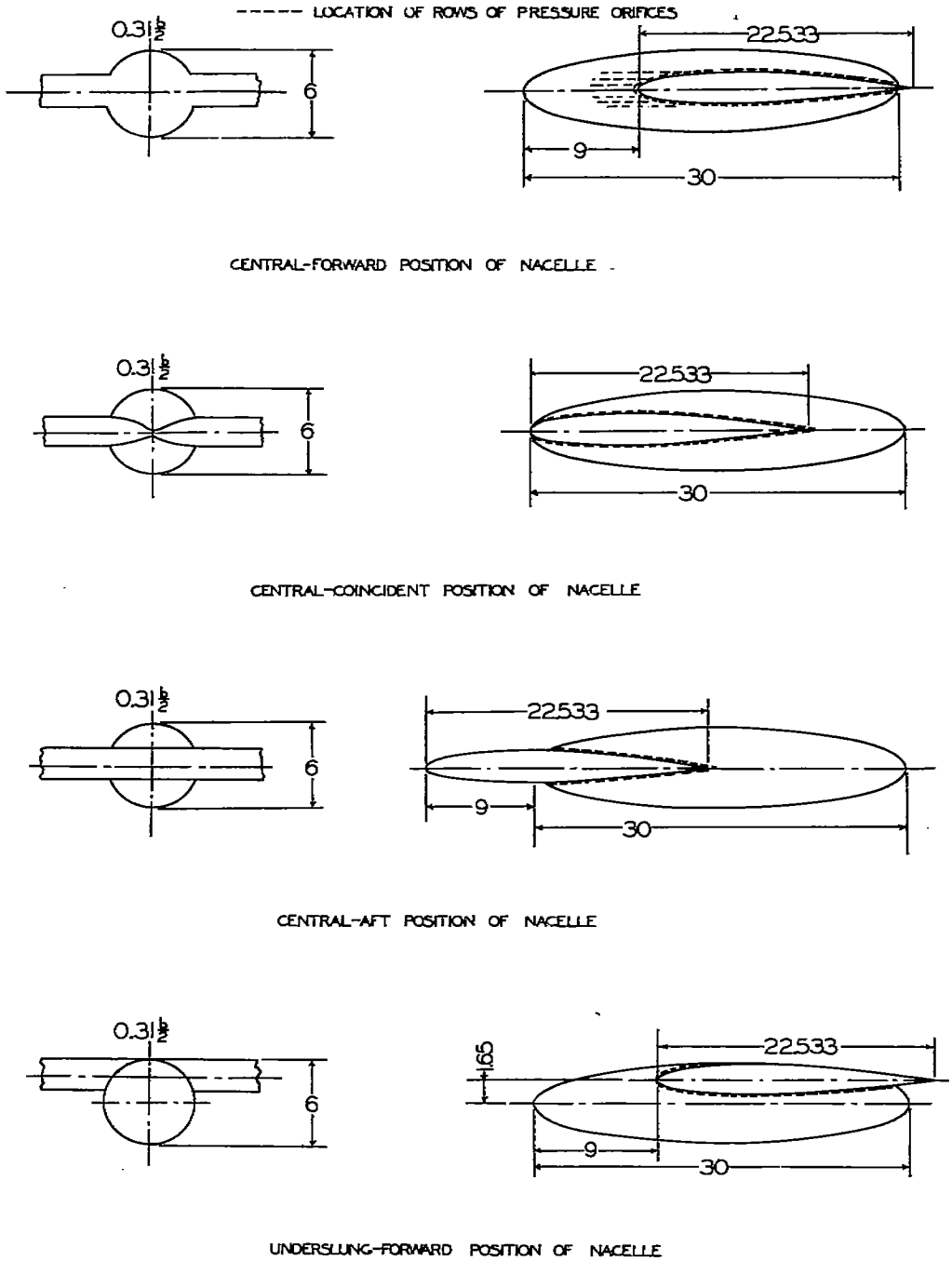

(a) NACELLE ON WING.

FIGURE 3.– POSITIONS OF NACELLE. (ALL DIMENSIONS ARE IN INCHES.)

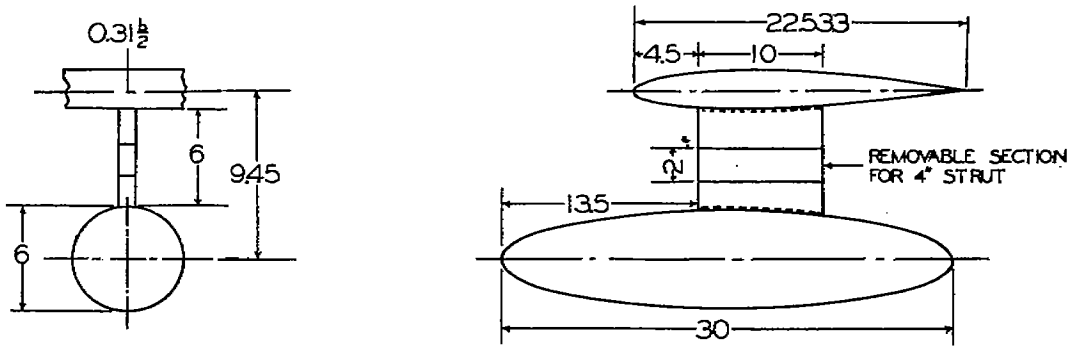

UNDERSLUNG-FORWARD POSITION OF NACELLE ON STRUT

- - - - - LOCATION OF ROWS OF PRESSURE ORIFICES

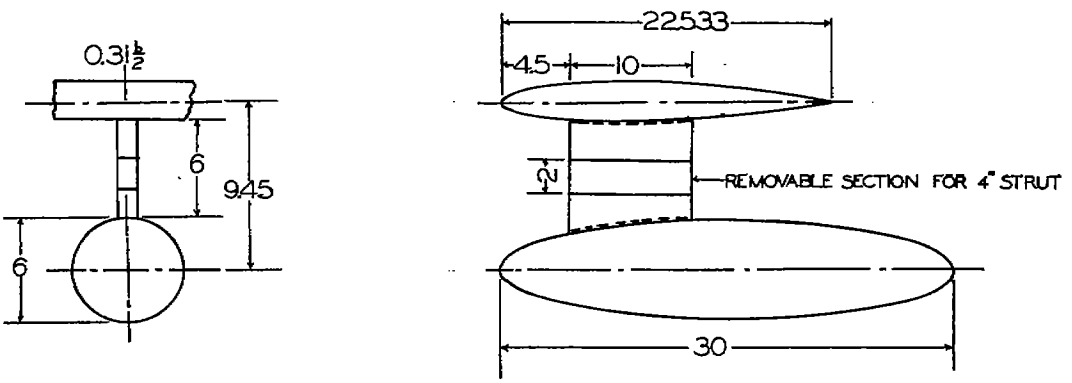

UNDERSLUNG-COINCIDENT POSITION OF NACELLE ON STRUT

(b) NACELLE ON STRUT.

FIGURE 3.—CONCLUDED.

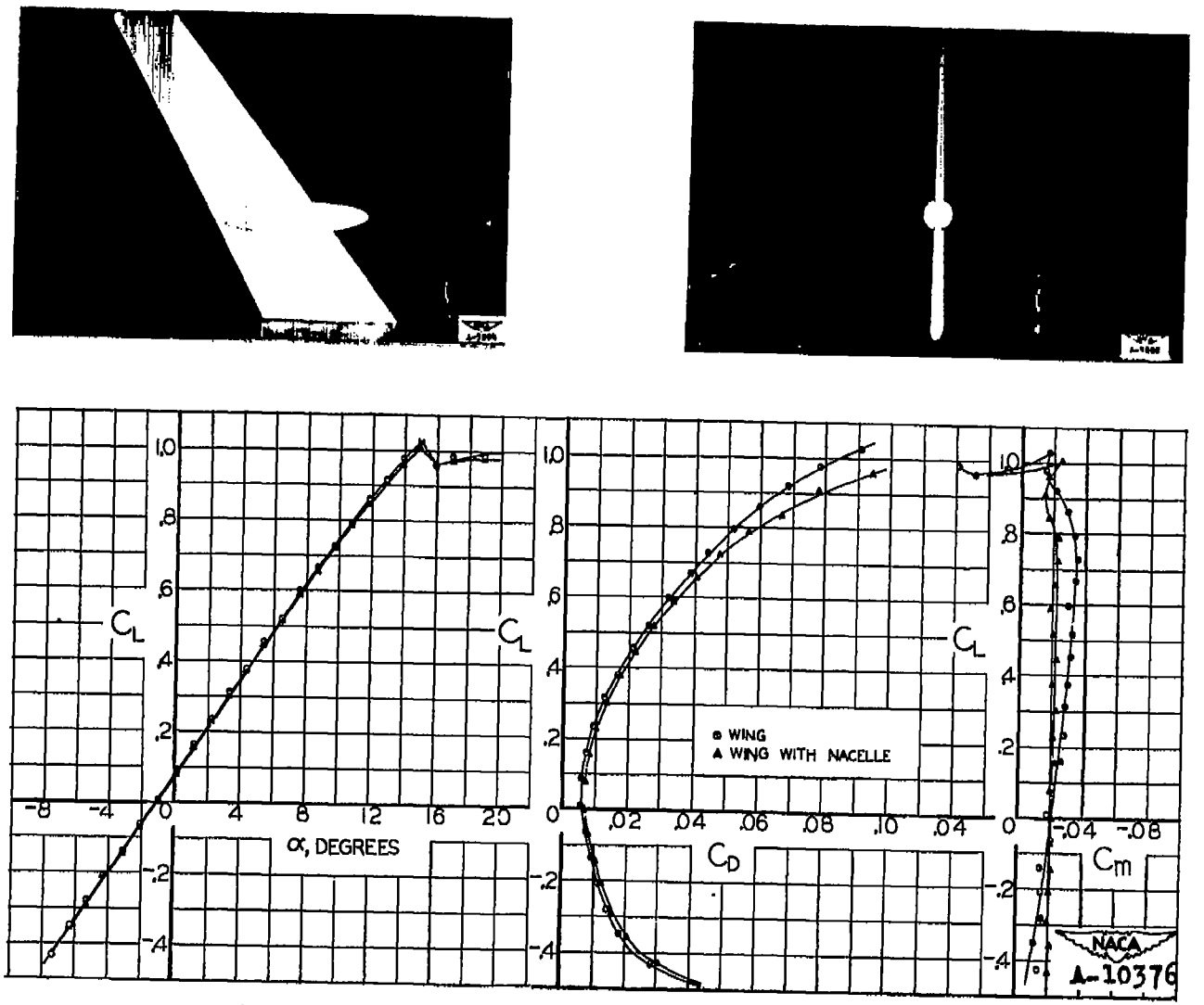

(a) Central-forward position of nacelle.

Figure 4.- Effect of the nacelle on the aerodynamic characteristics of the wing.

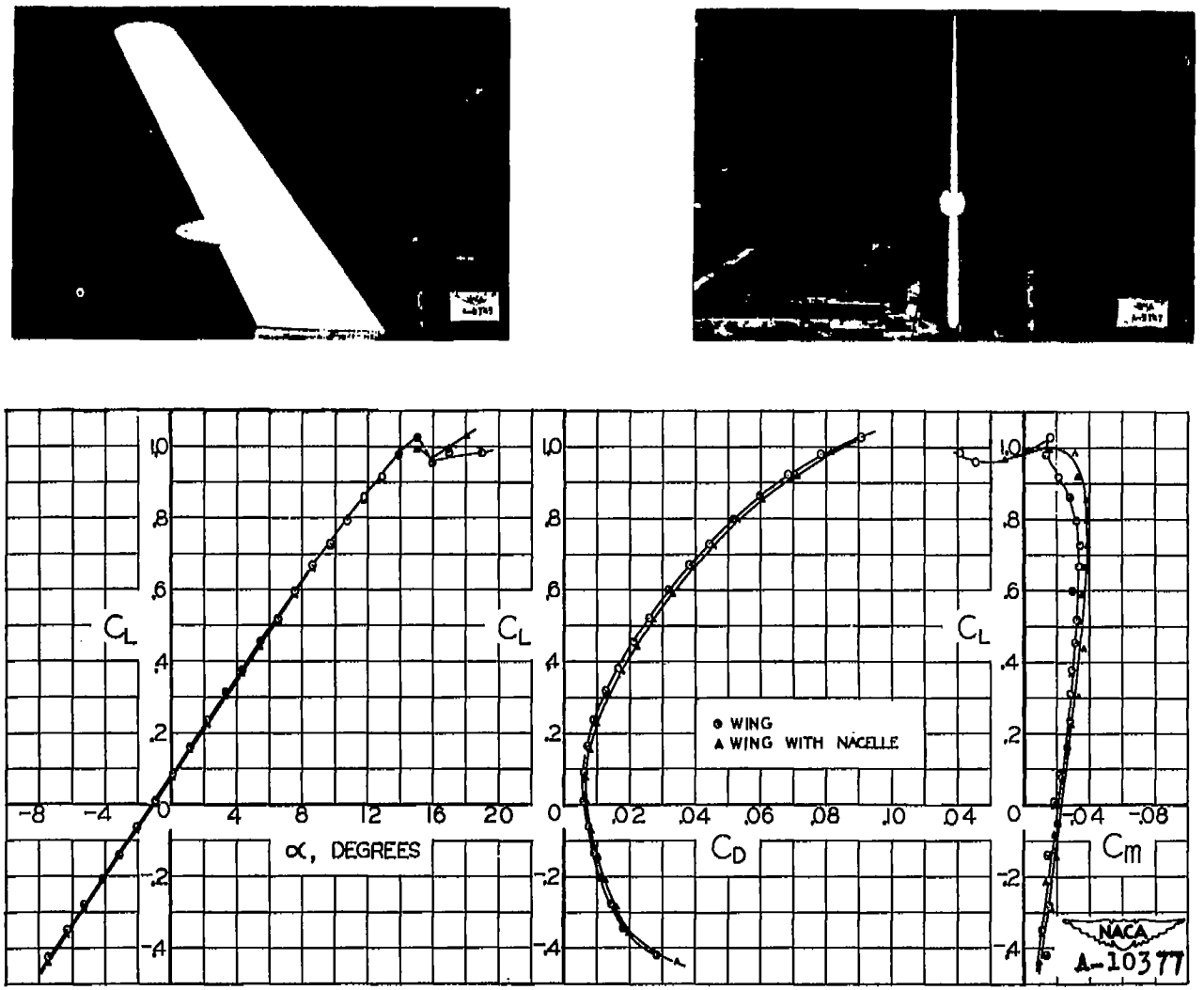

(b) Central-coincident position of nacelle.
Figure 4.- Continued.

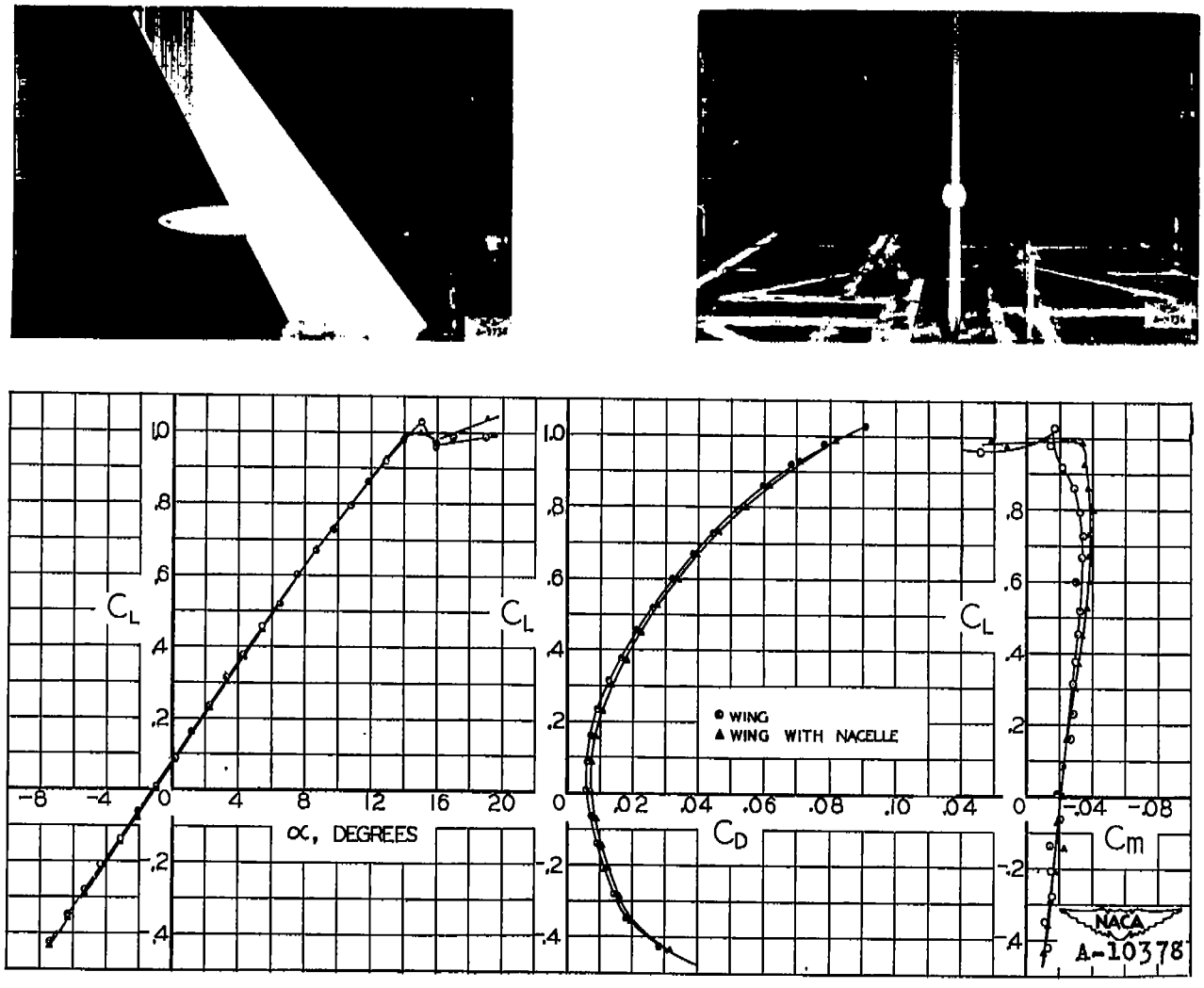

(c) Central-aft position of nacelle.
Figure 4.- Continued.

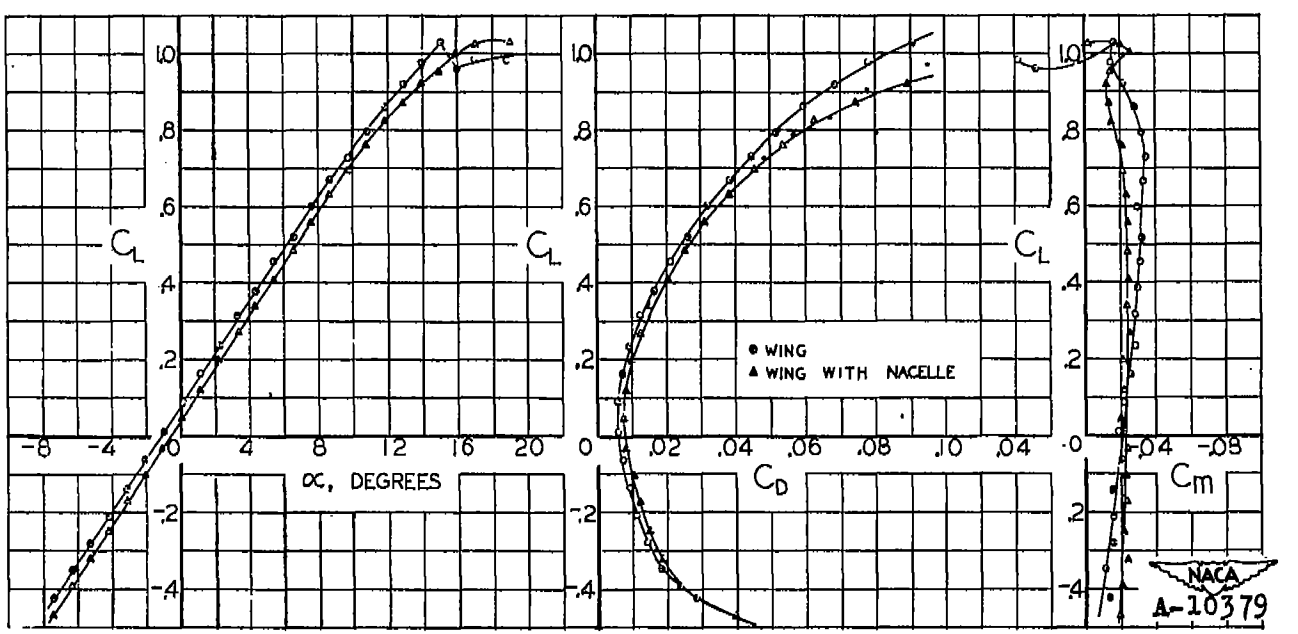

(d) Underslung-forward position of nacelle.
Figure 4.- Continued.

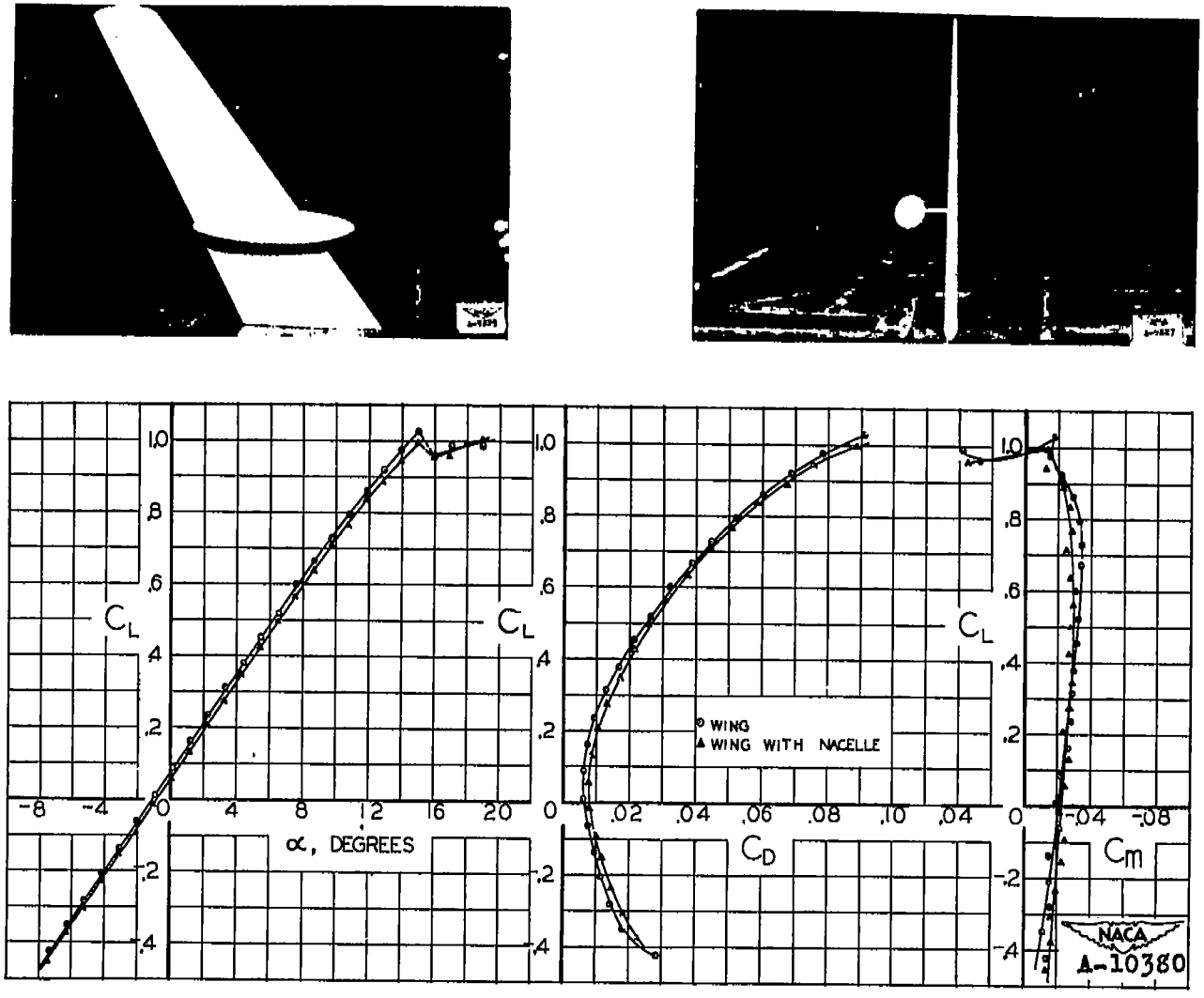

(e) Underslung-forward position of nacelle on a 4-inch strut.
Figure 4.- Continued.

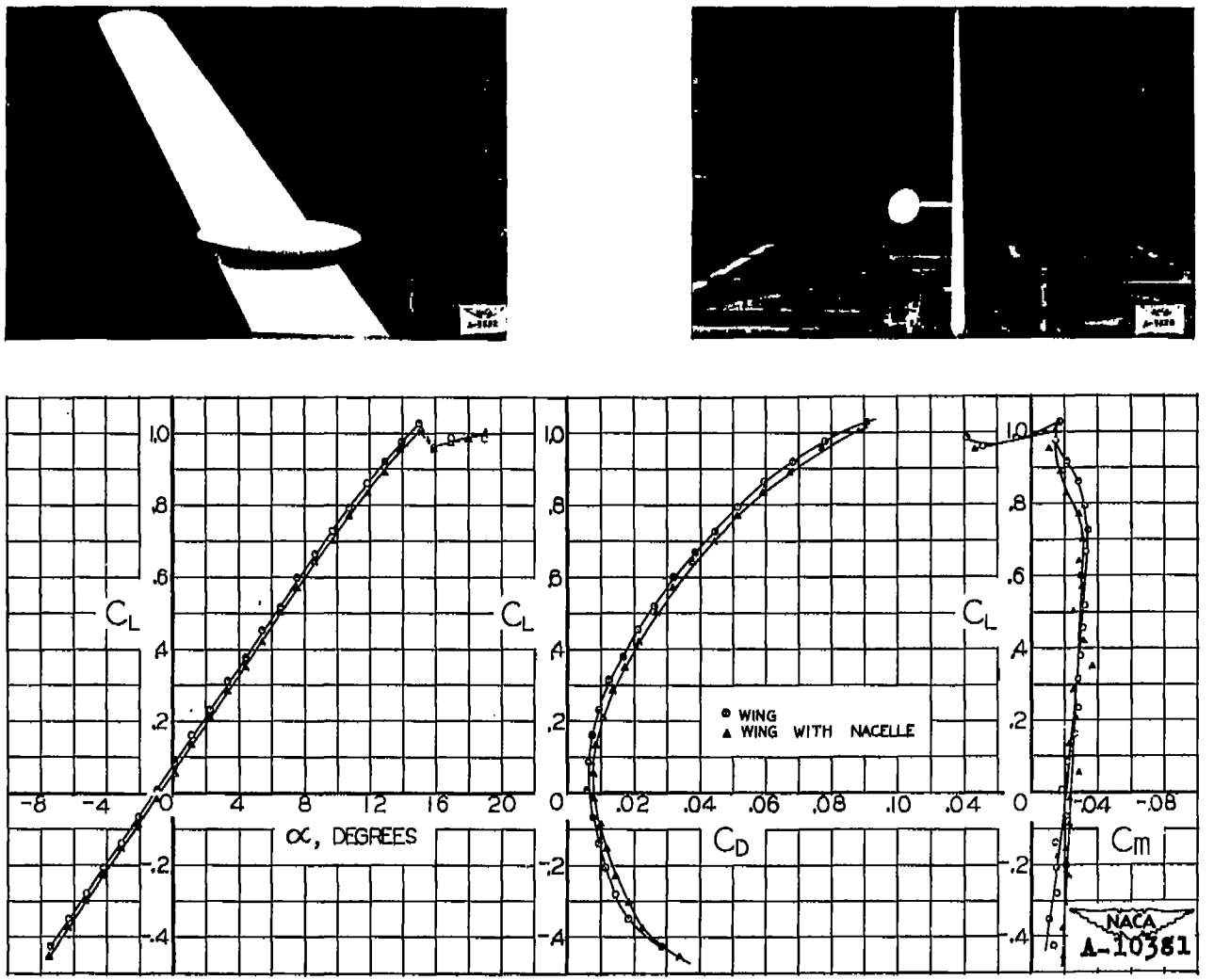

(f) Underslung-forward position of nacelle on a 6-inch strut.
Figure 4.– Continued.

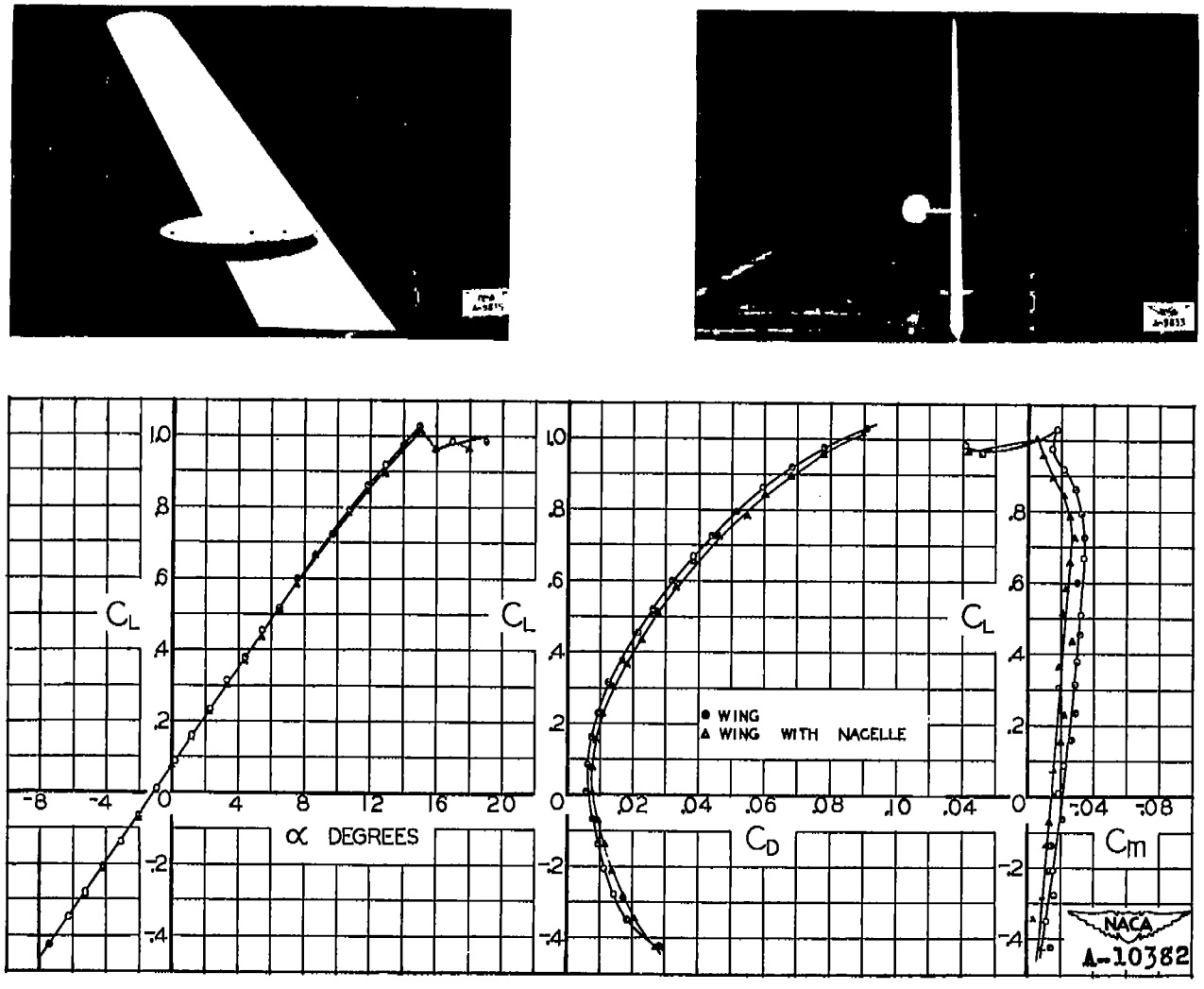

(g) Underslung-coincident position of nacelle on a 4-inch strut.
Figure 4.- Continued.

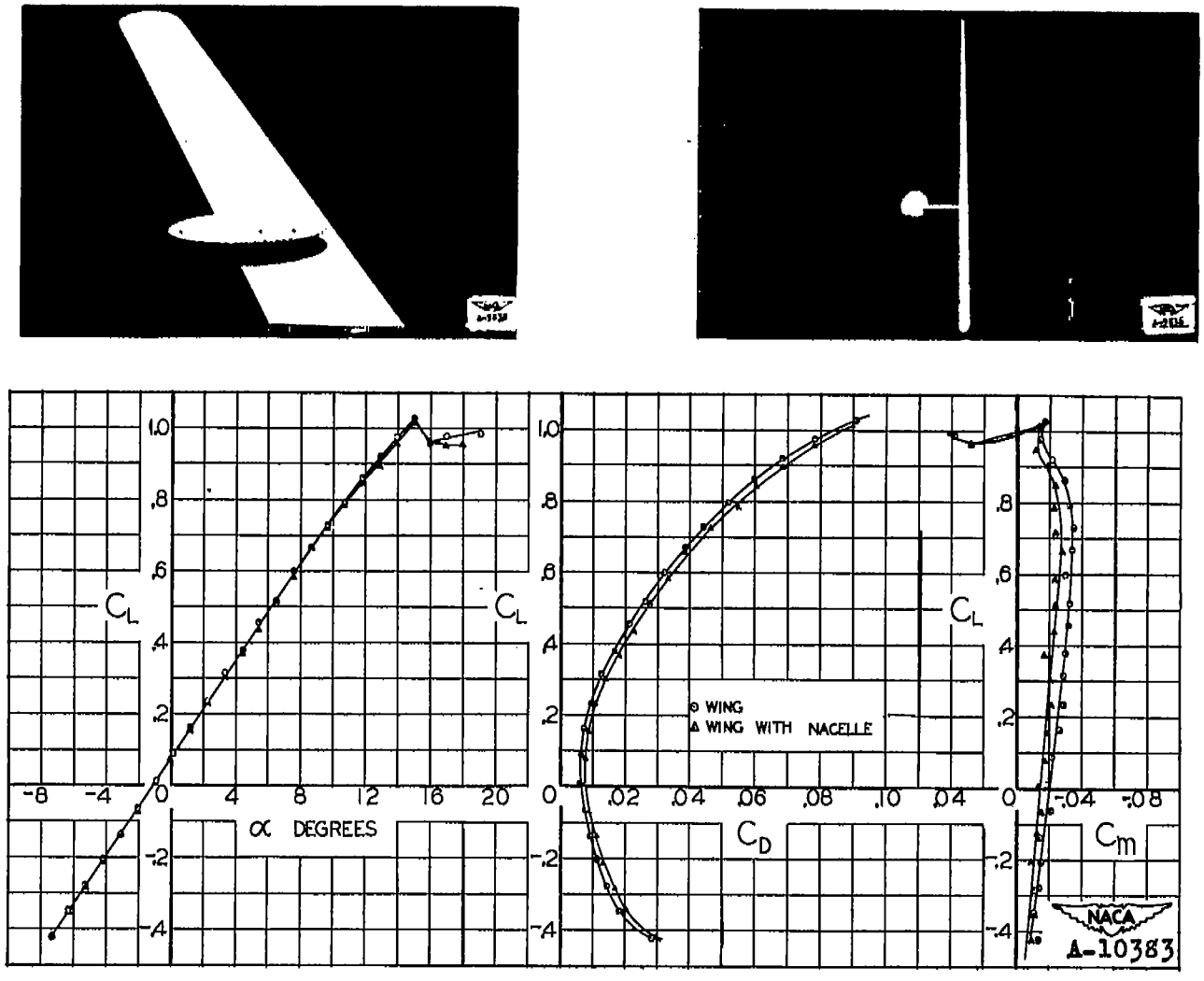

(h) Underslung-coincident position of nacelle on a 6-inch strut.
Figure 4.- Concluded.

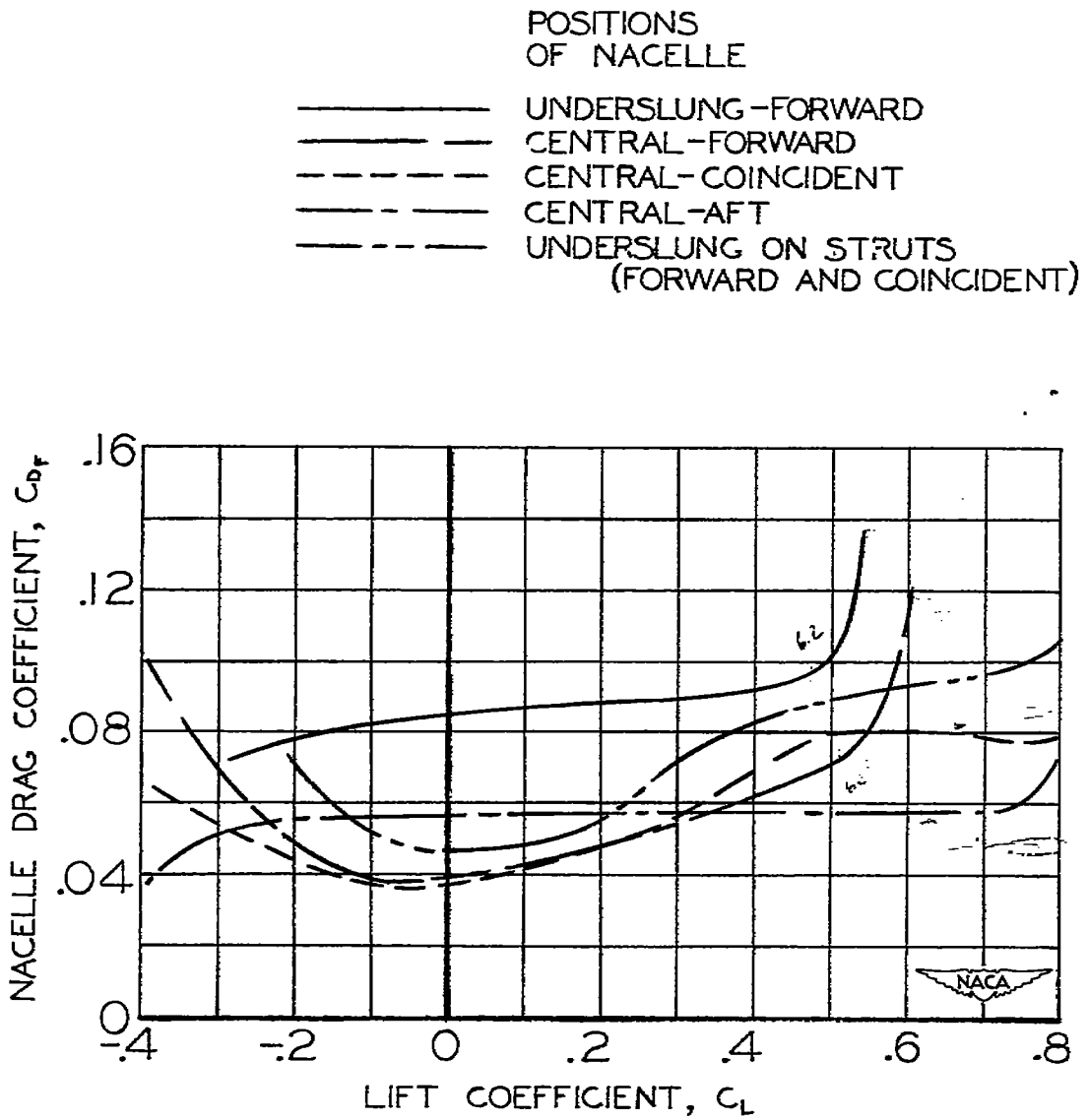

FIGURE 5.- THE VARIATION OF THE DRAG COEFFICIENT OF THE NACELLE WITH LIFT COEFFICIENT FOR THE VARIOUS NACELLE POSITIONS.

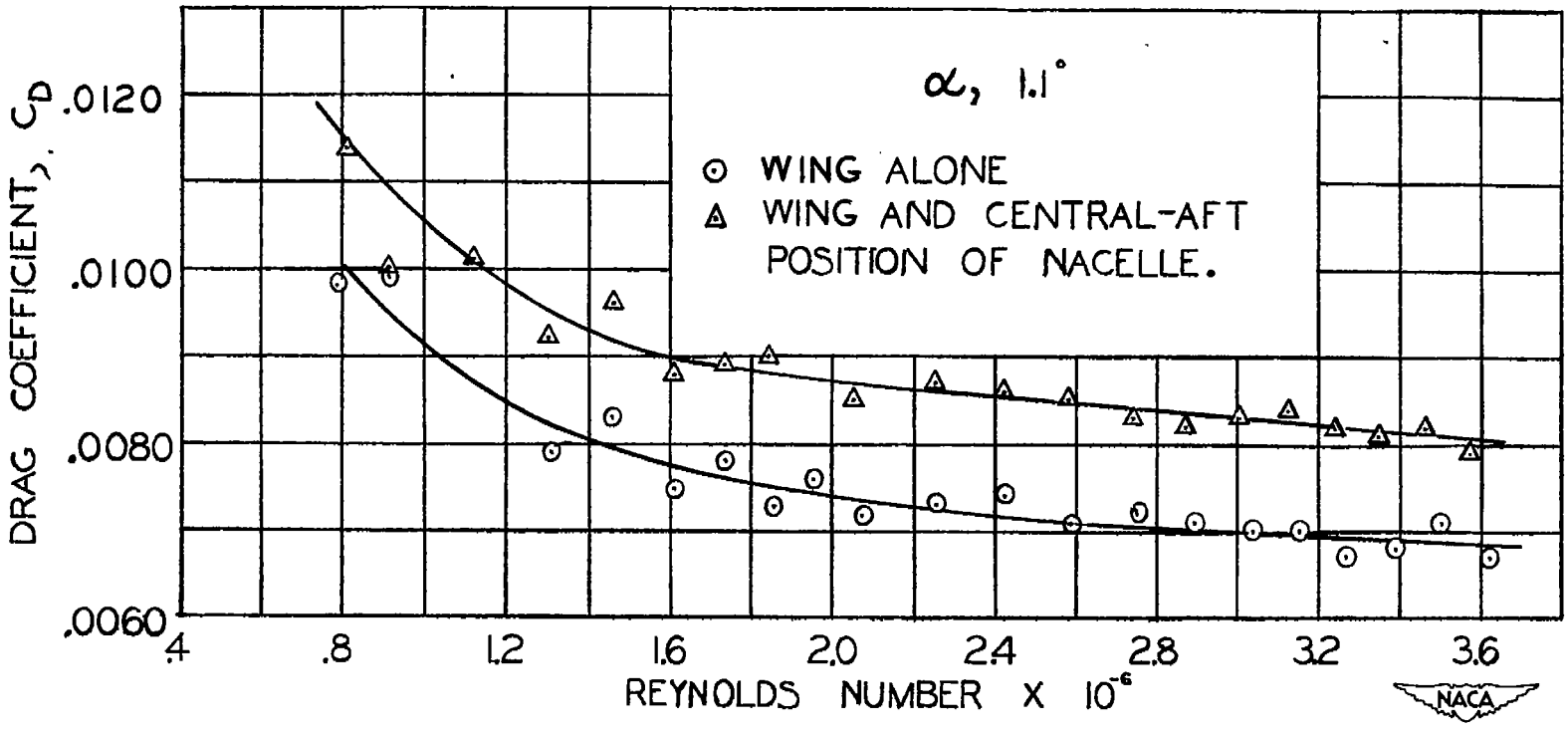

FIGURE 6.- VARIATION OF DRAG COEFFICIENT WITH REYNOLDS NUMBER.

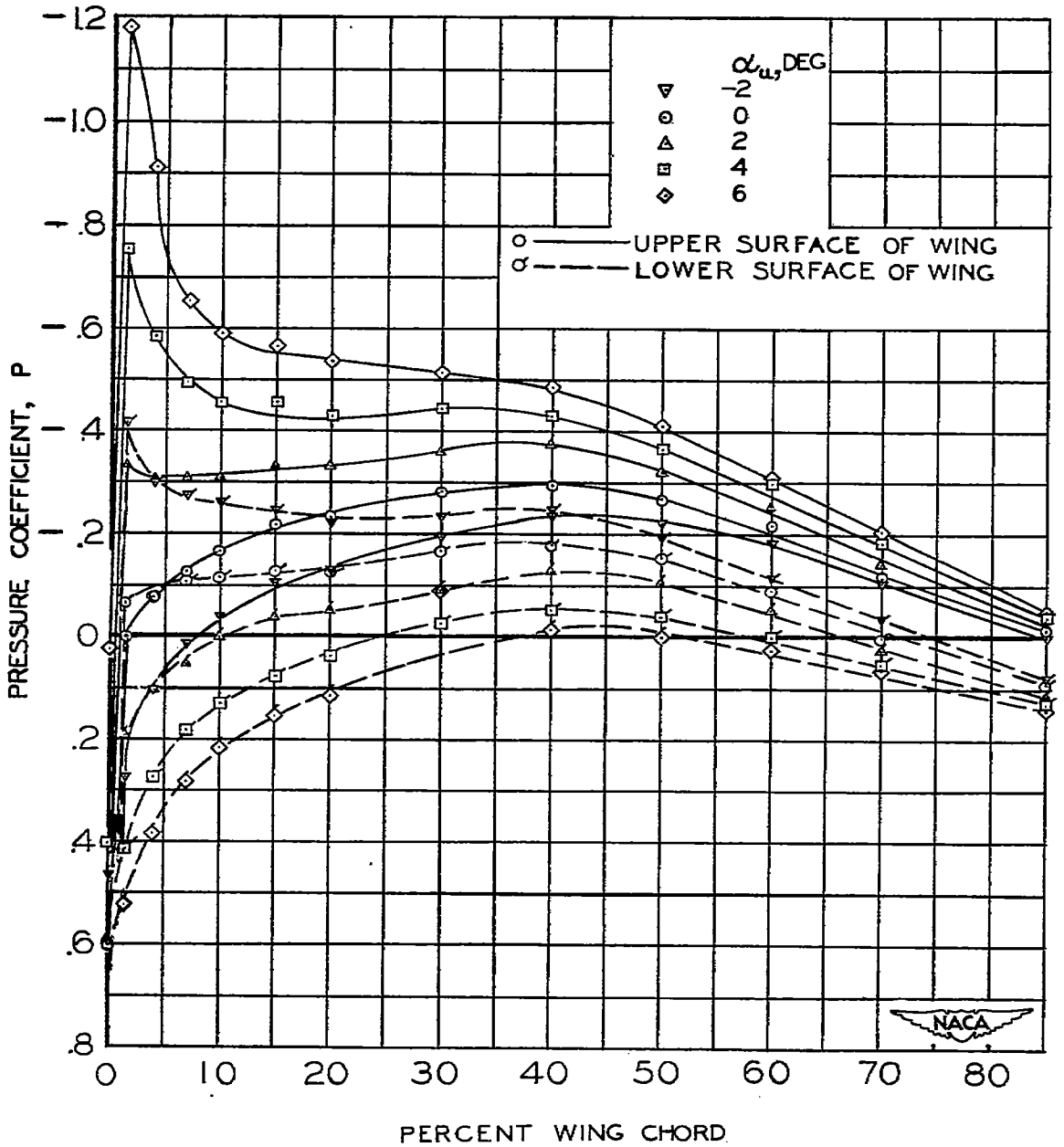

(a) 15-PERCENT SEMISPAN

FIGURE 7.- CHORDWISE PRESSURE DISTRIBUTIONS AT VARIOUS SPANWISE STATIONS ON THE WING ALONE.

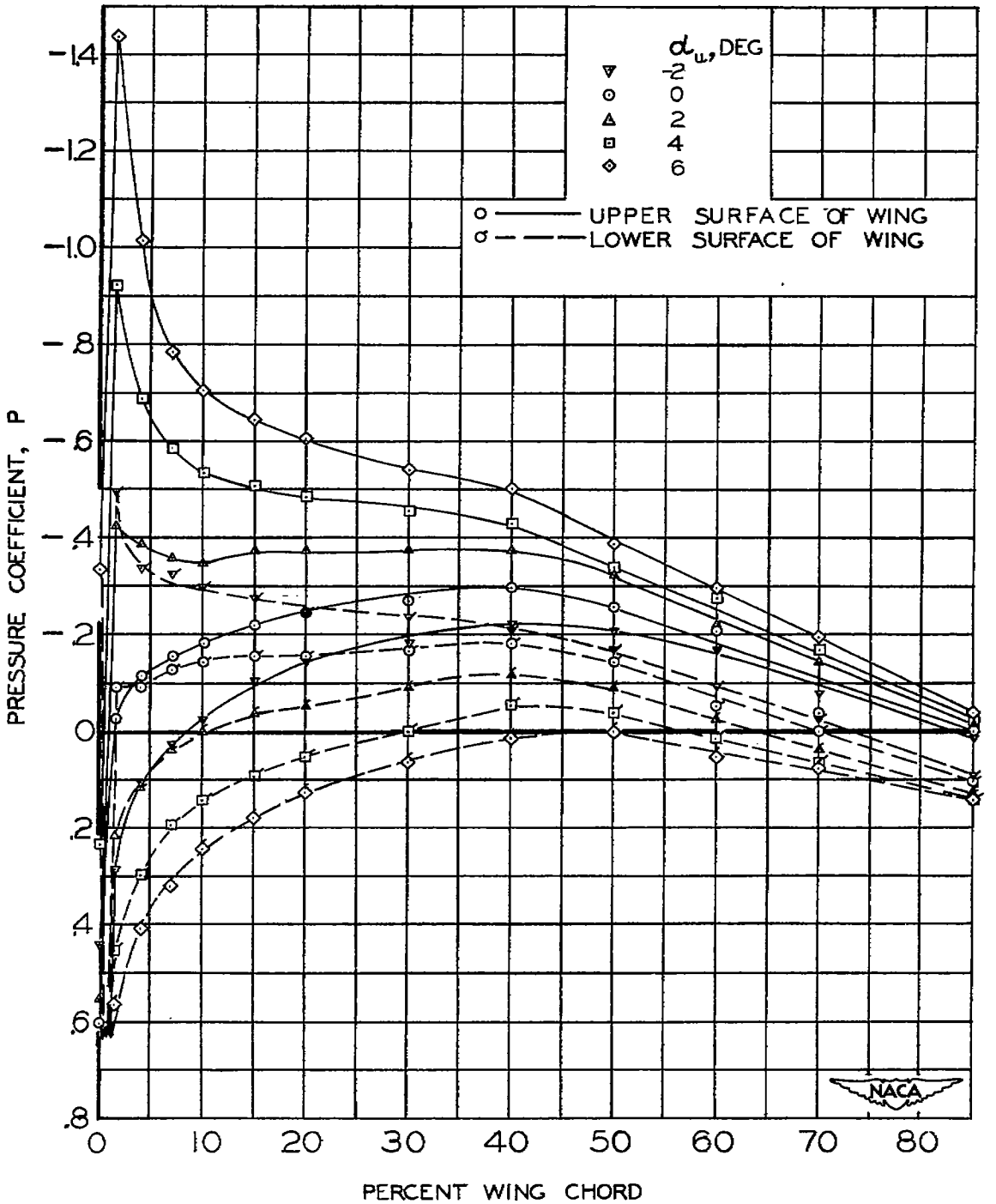

(b) 31-PERCENT SEMISPAN

FIGURE 7.- CONTINUED

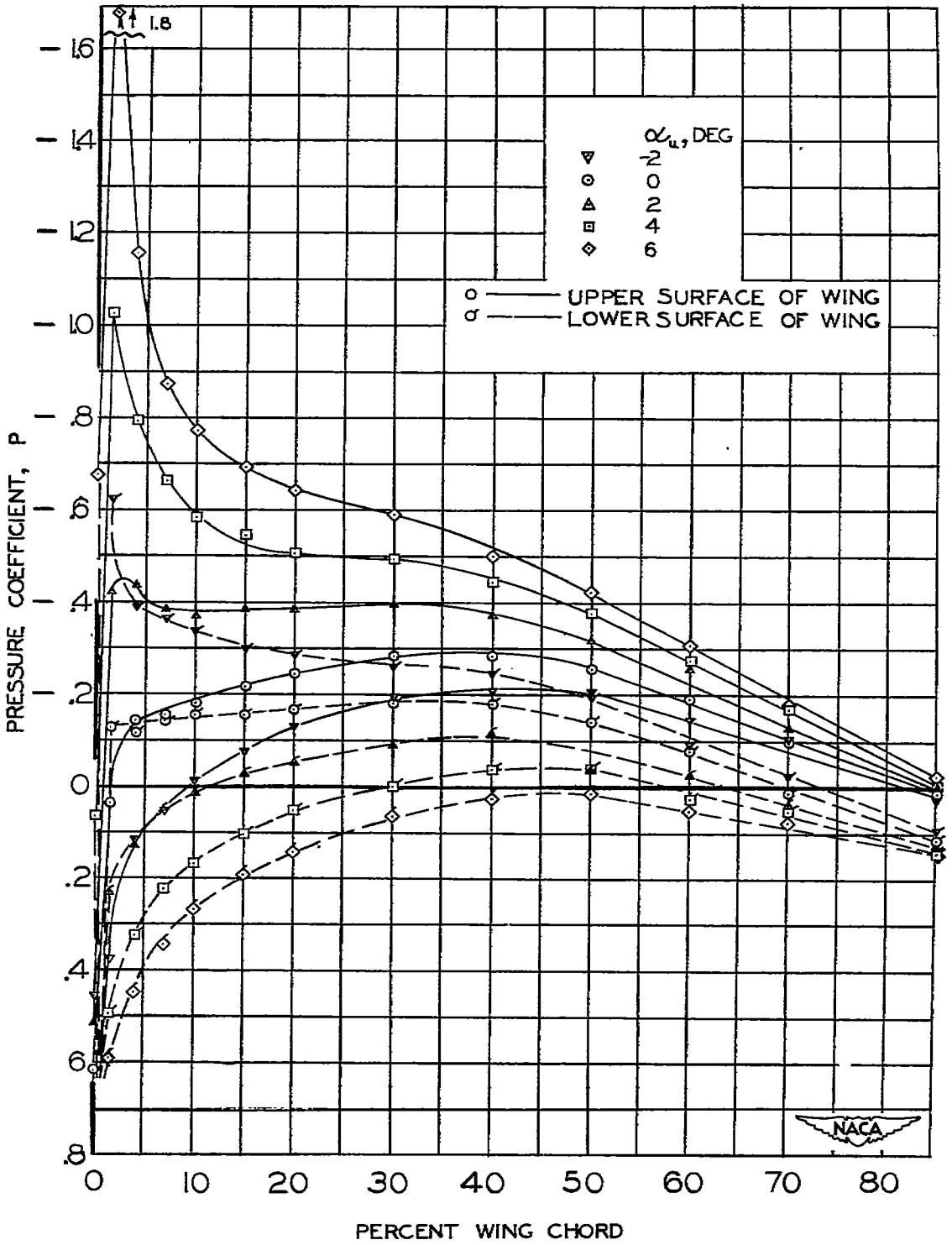

(c) 55-PERCENT SEMISPAN

FIGURE 7.- CONTINUED

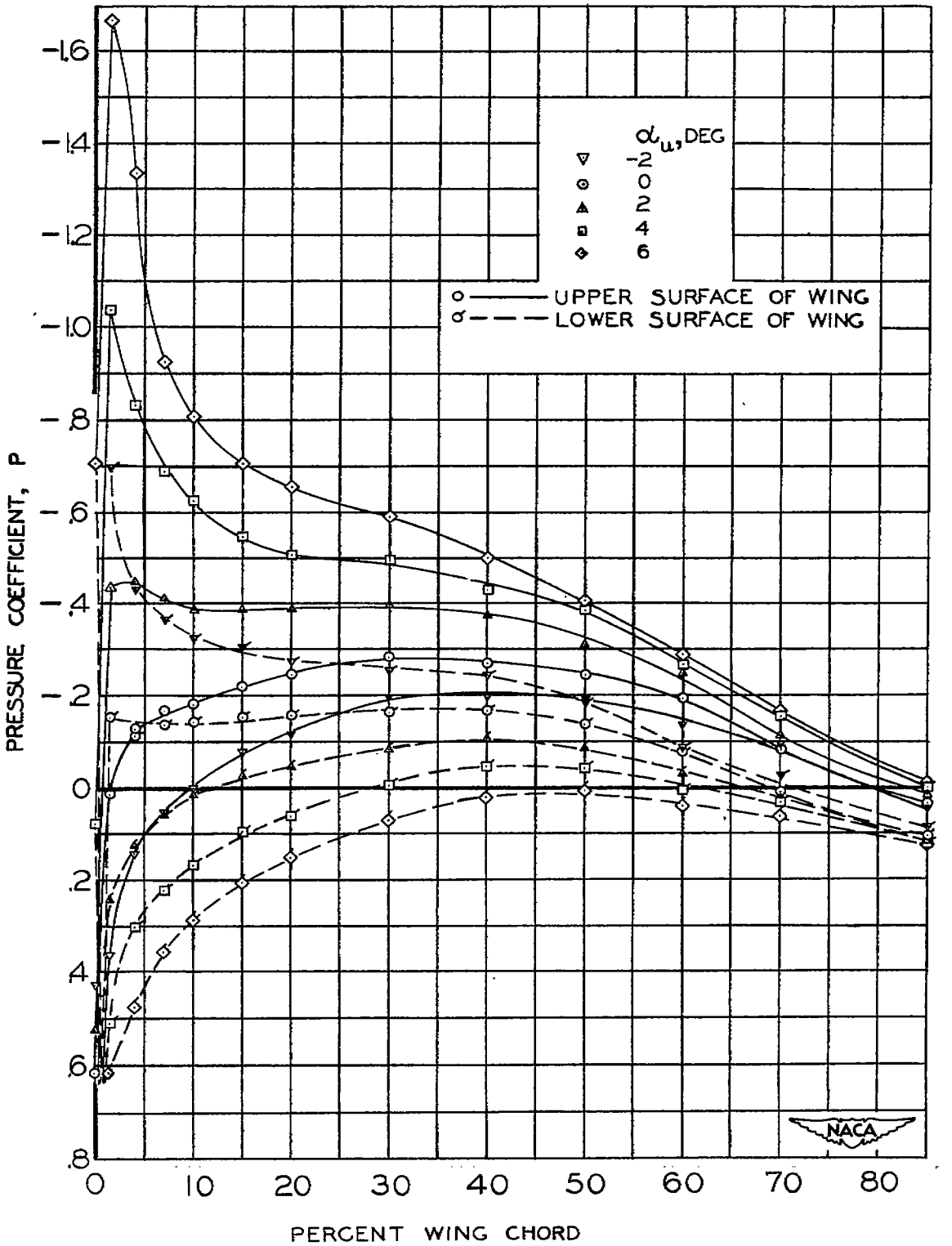

(d) 73.3-PERCENT SEMISPAN

FIGURE 7.- CONTINUED

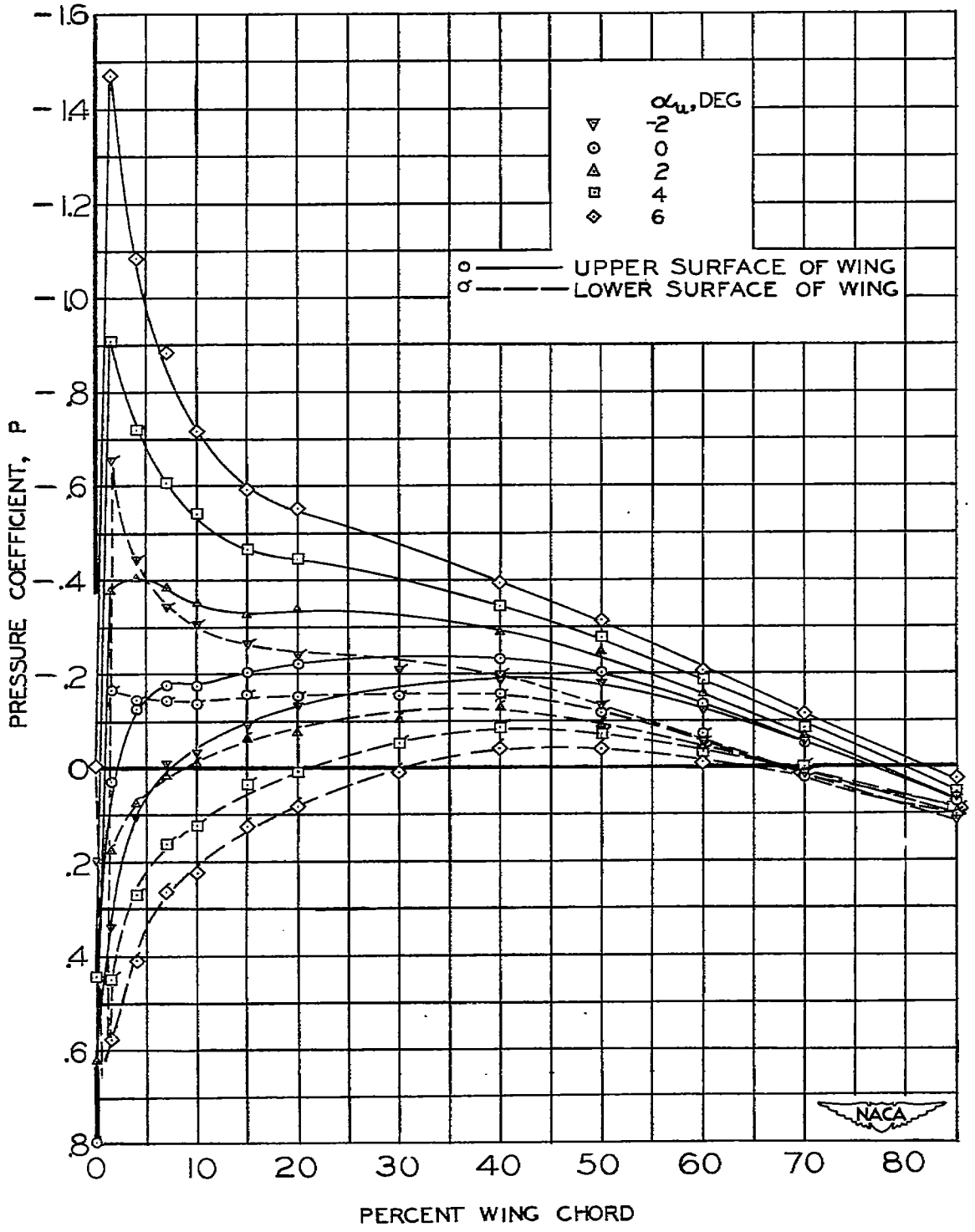

(e) 91.7 - PERCENT SEMISPAN

FIGURE 7.- CONCLUDED

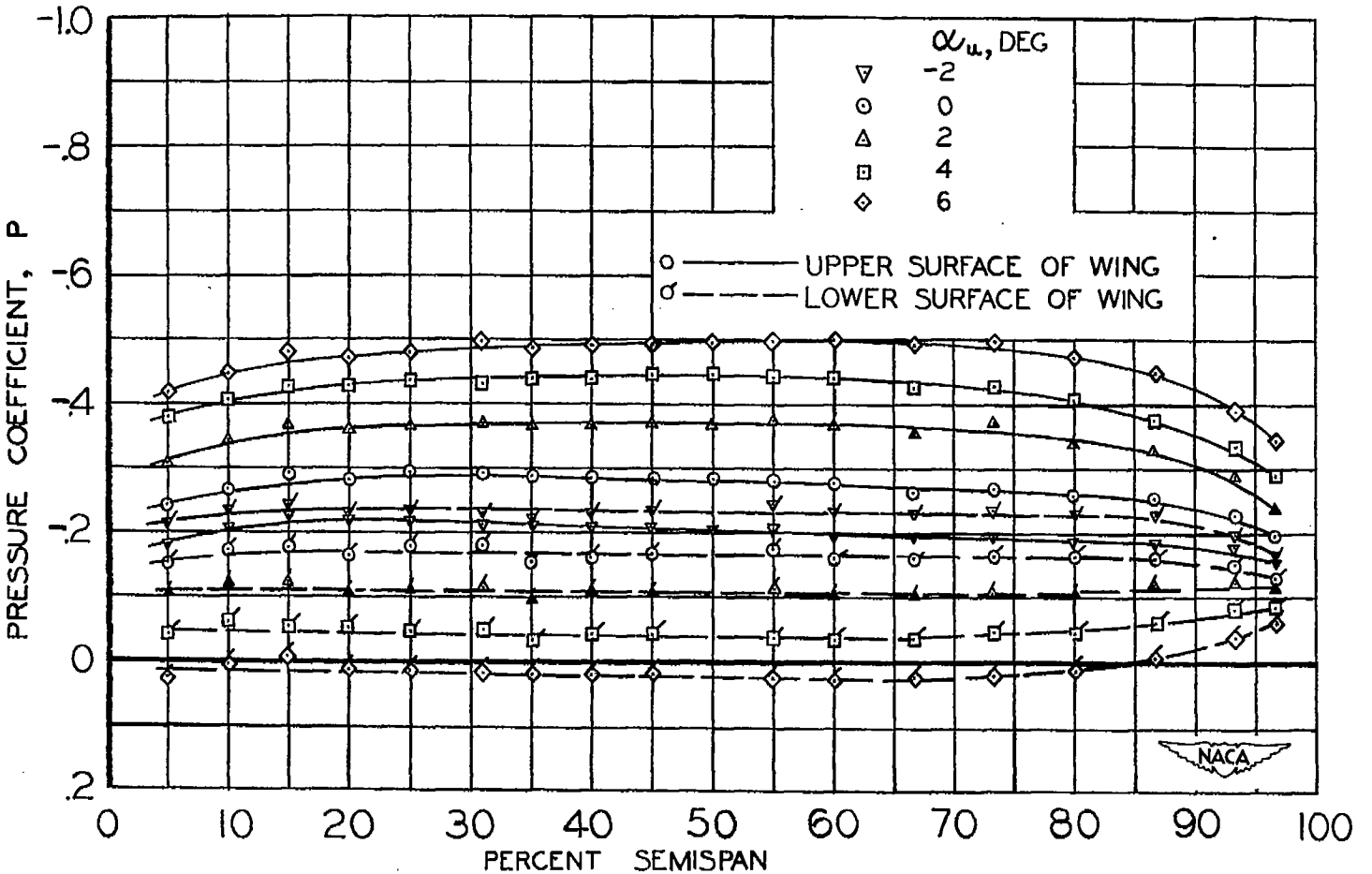

FIGURE 8. - SPANWISE PRESSURE DISTRIBUTION AT 40-PERCENT OF THE CHORD OF THE WING ALONE.

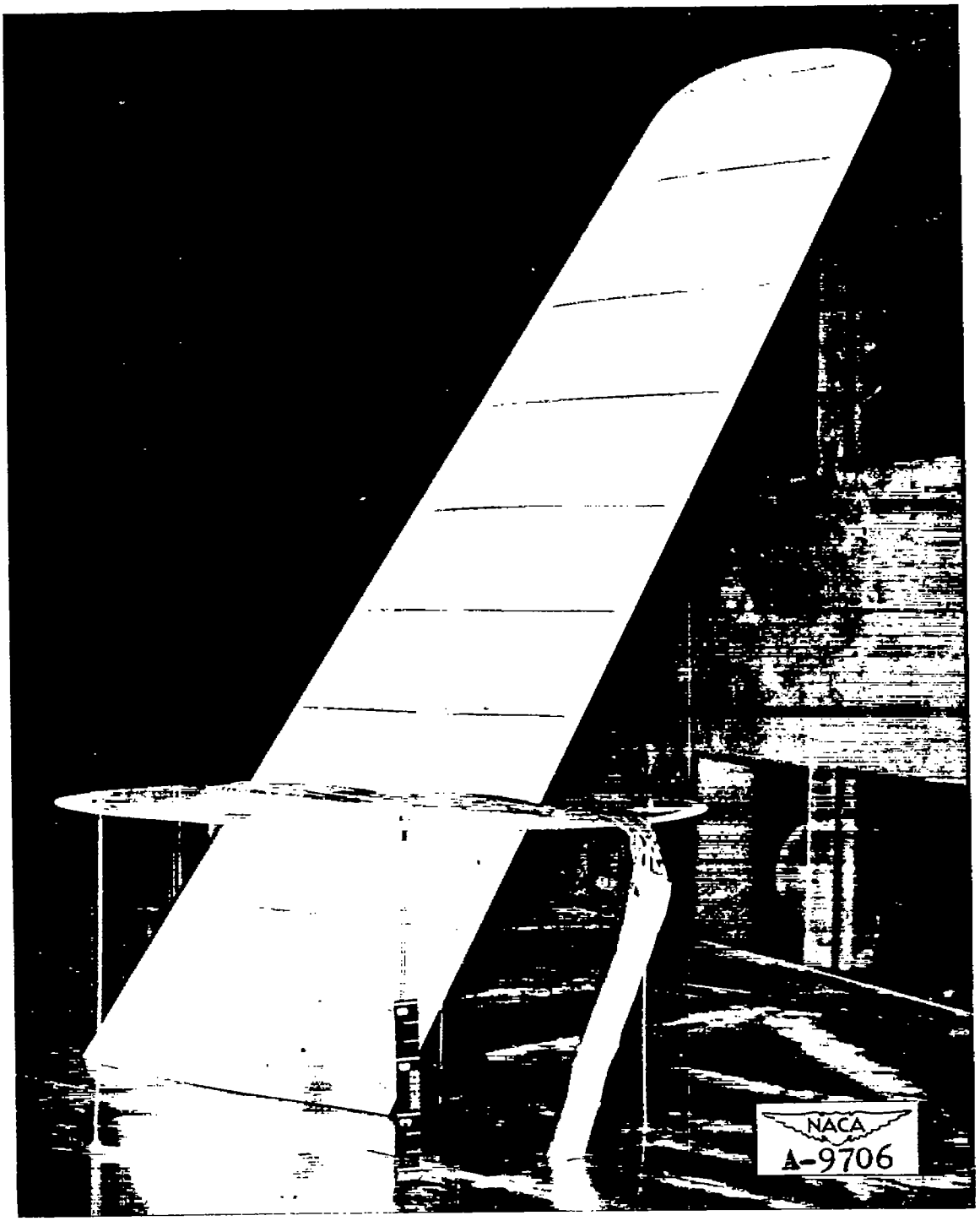

Figure 9.– Three-foot diameter flat plate at 31-percent semispan of the wing.

Wing Span/chord = 1.60

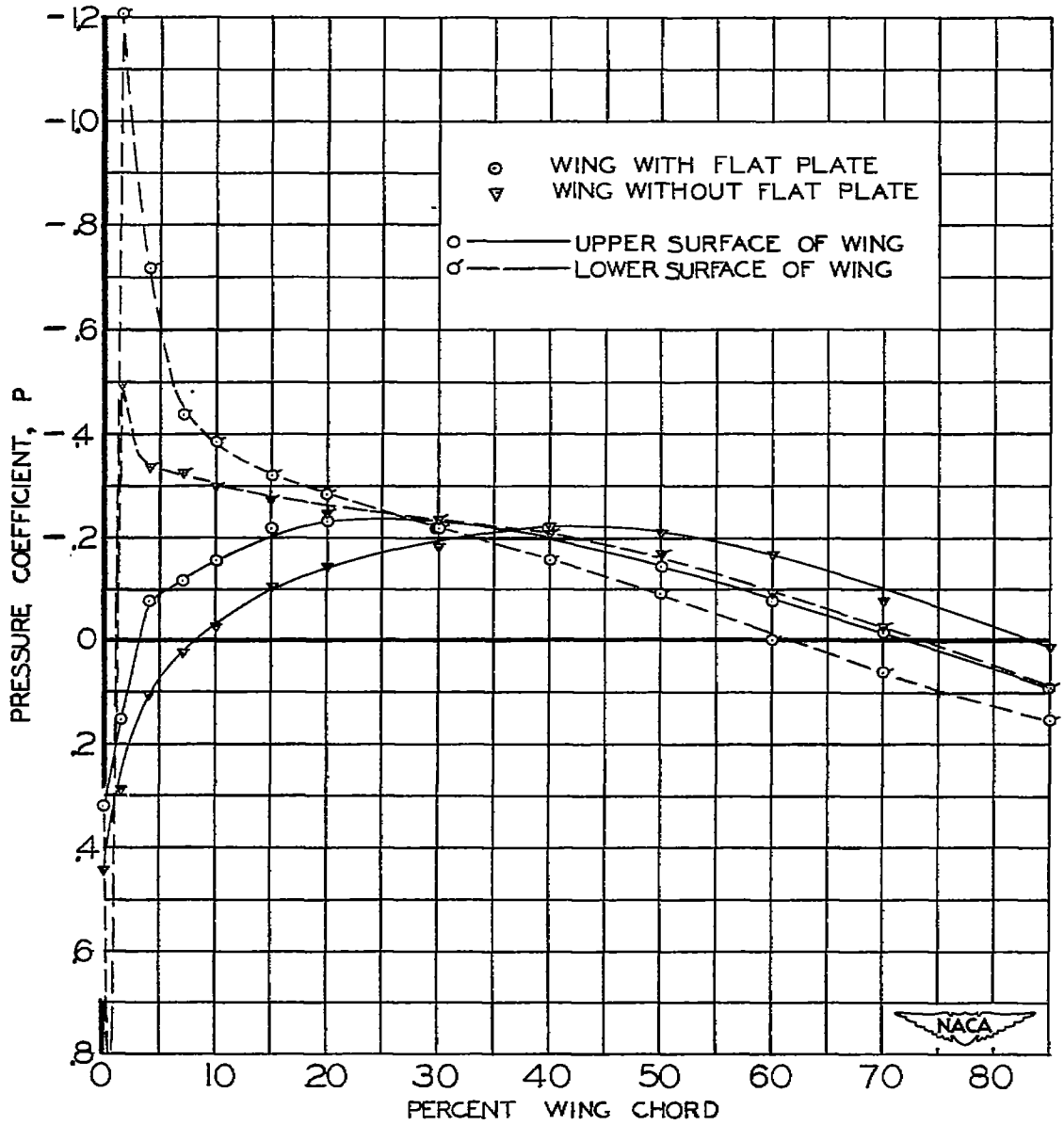

(a) $\alpha_u, -2^\circ$

FIGURE 10.-CHORDWISE PRESSURE DISTRIBUTION ON THE INBOARD JUNCTURE OF THE WING AND THE FLAT PLATE PARALLEL TO THE PLANE OF SYMMETRY.

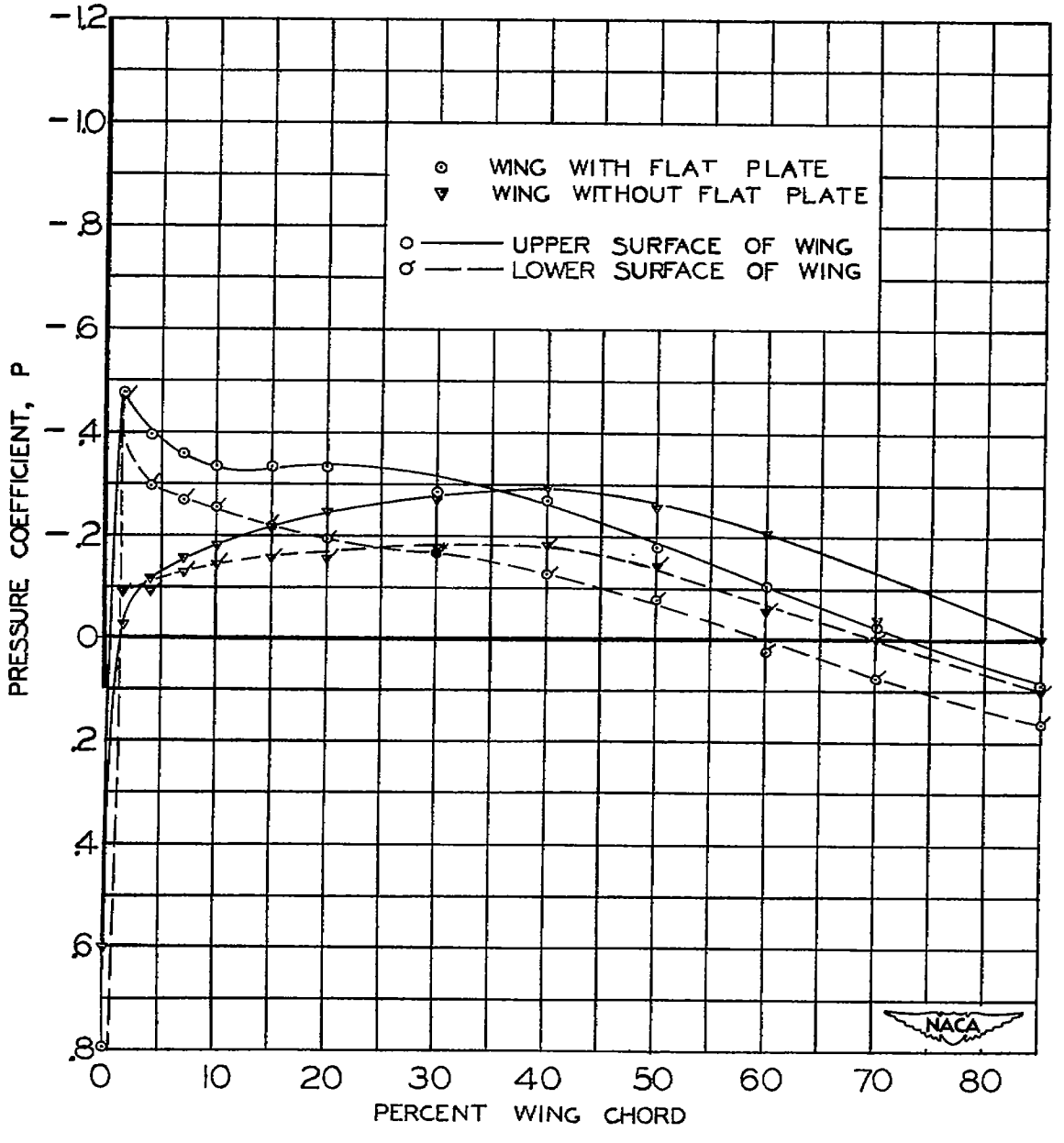

(b) $\alpha_u, 0°$

FIGURE 10 - CONTINUED

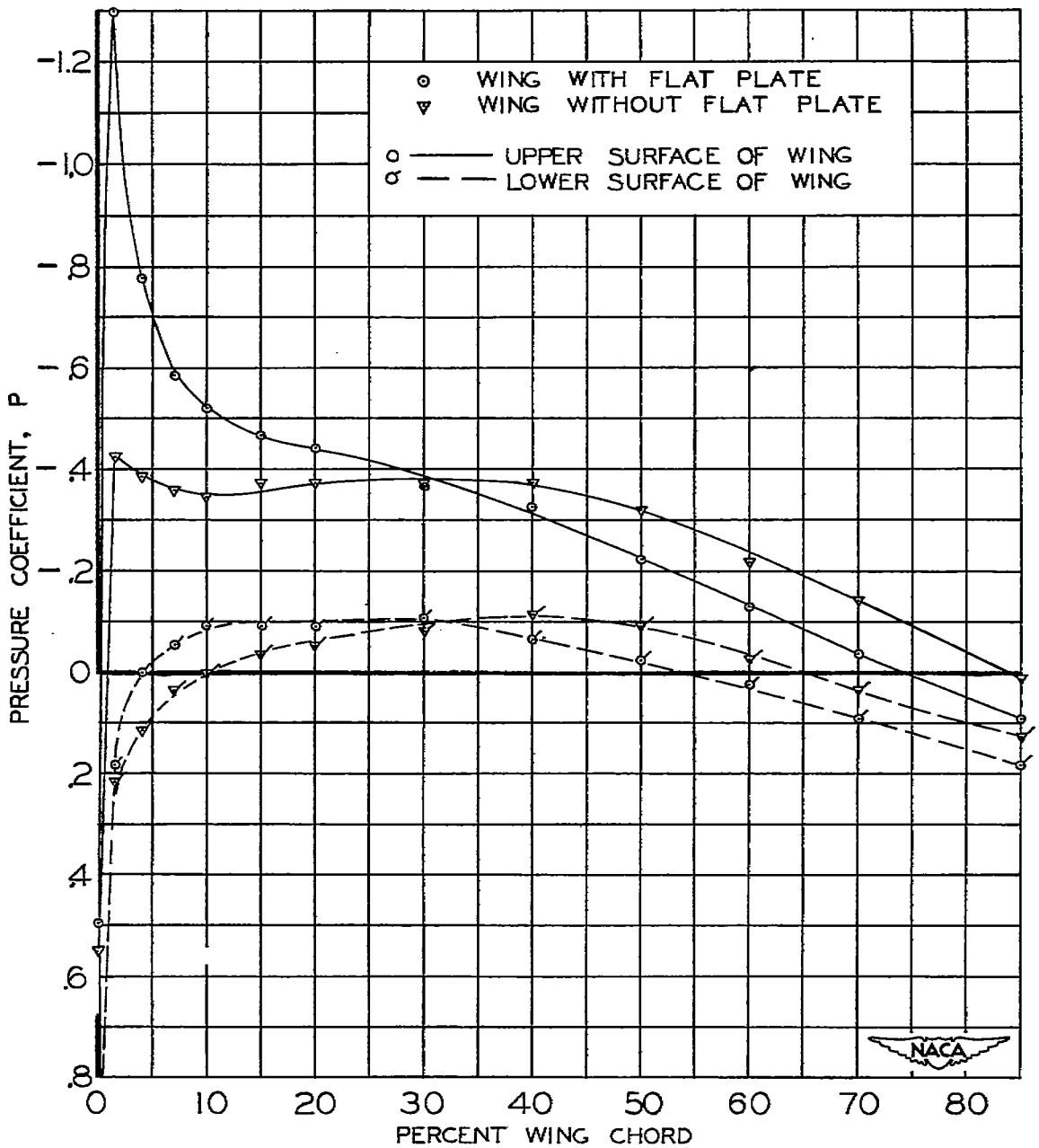

(c) α_u, 2°

FIGURE 10. - CONTINUED

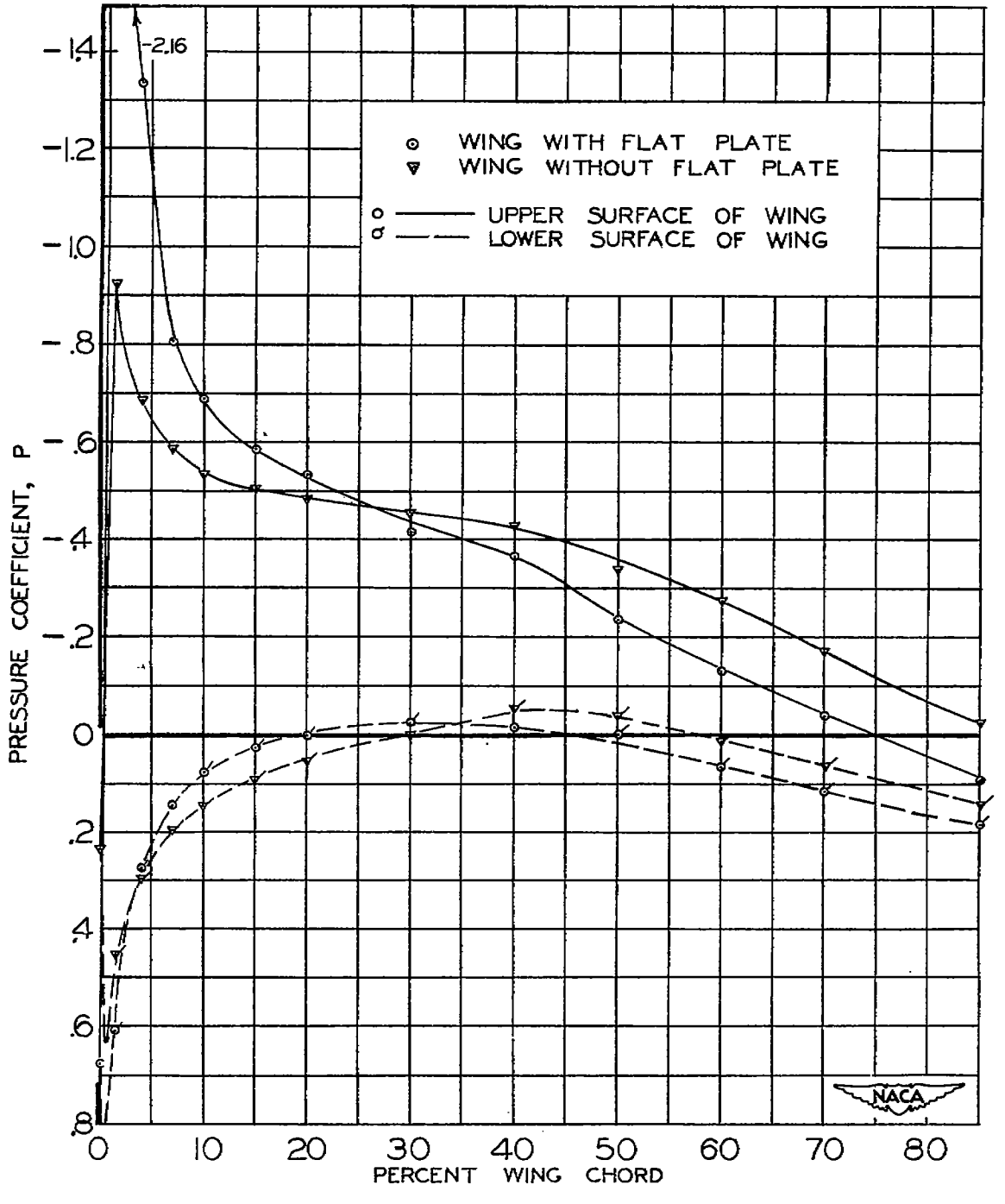

(d) α_u, 4°

FIGURE 10. - CONTINUED

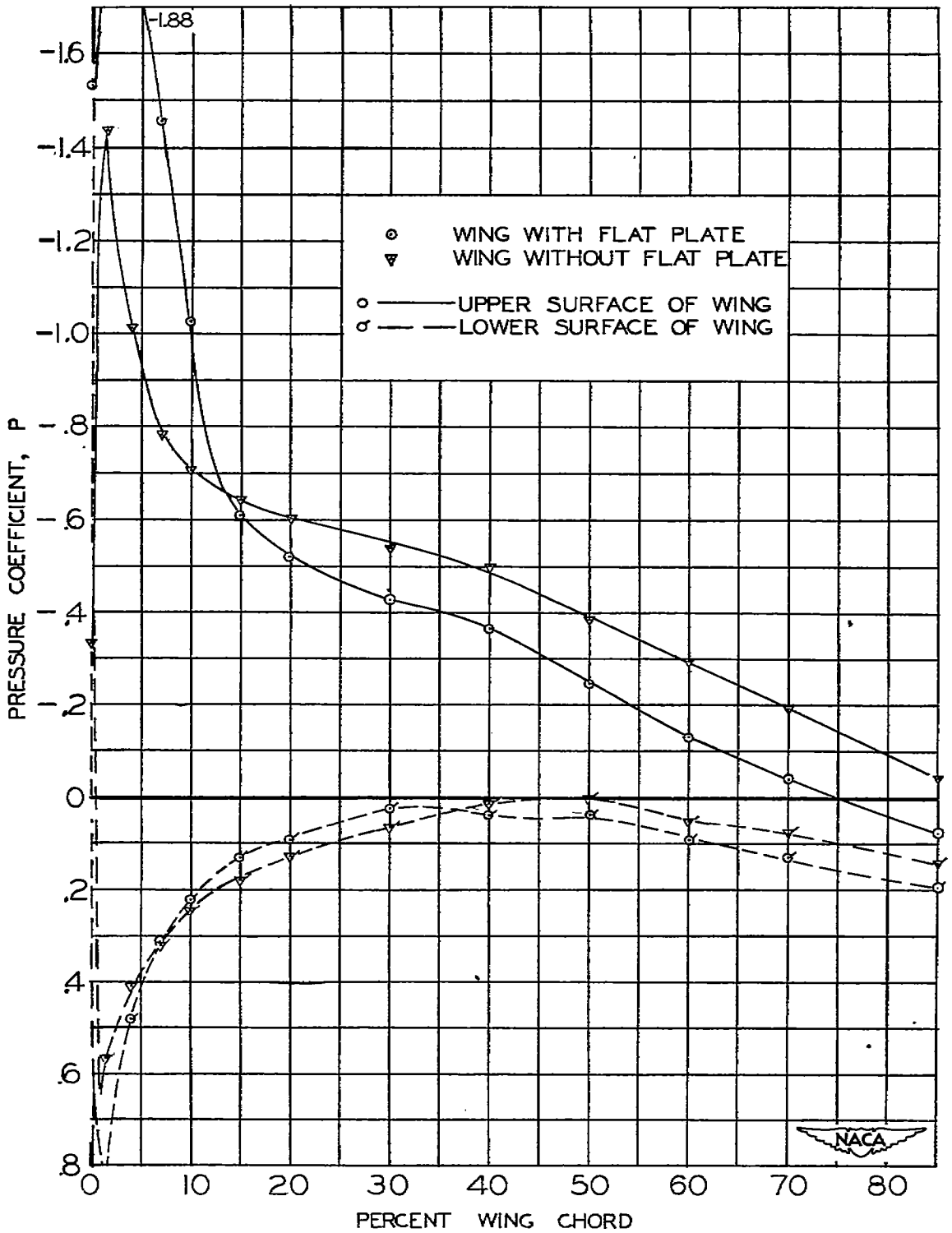

(e) α_u, 6°

FIGURE 10. - CONCLUDED

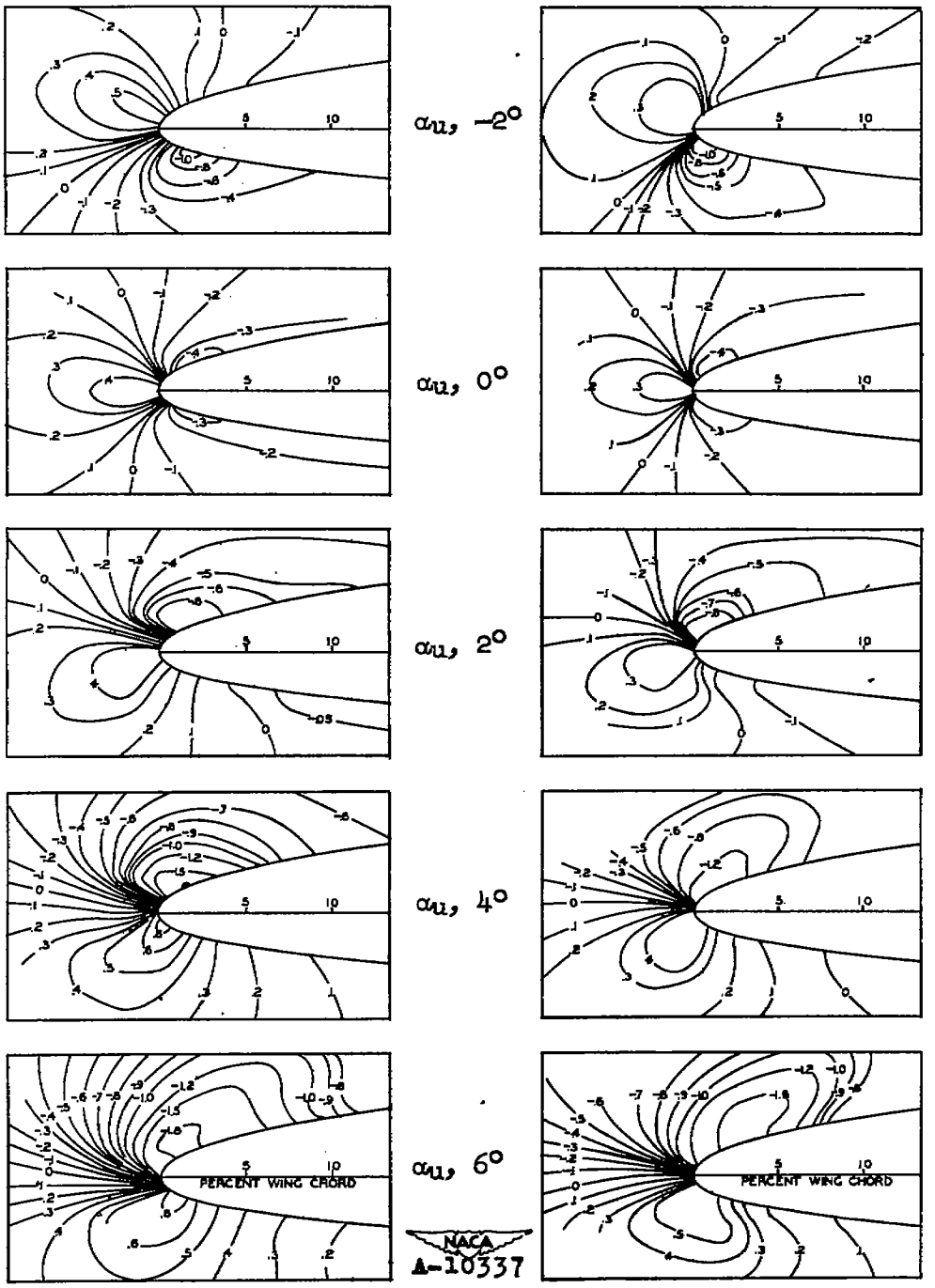

(a) Flat plate parallel to plane of symmetry.

(b) Central-forward position of nacelle.

Figure 11.– Contour lines of pressure coefficient near the leading edge of the wing with the flat plate and the nacelle on the wing.

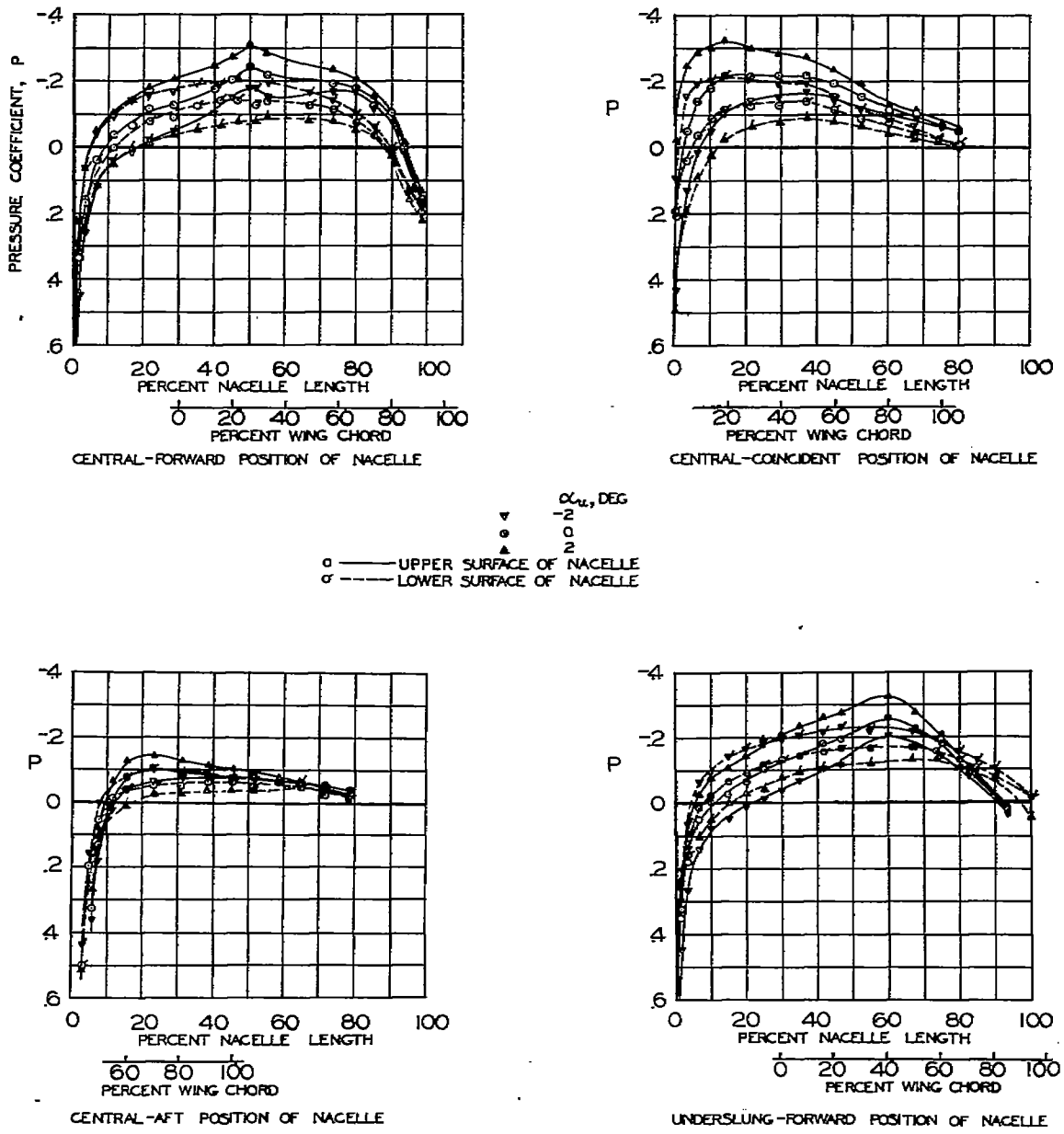

FIGURE 12.-PRESSURE DISTRIBUTIONS ALONG UPPER AND LOWER SURFACES OF THE NACELLE ON THE WING.

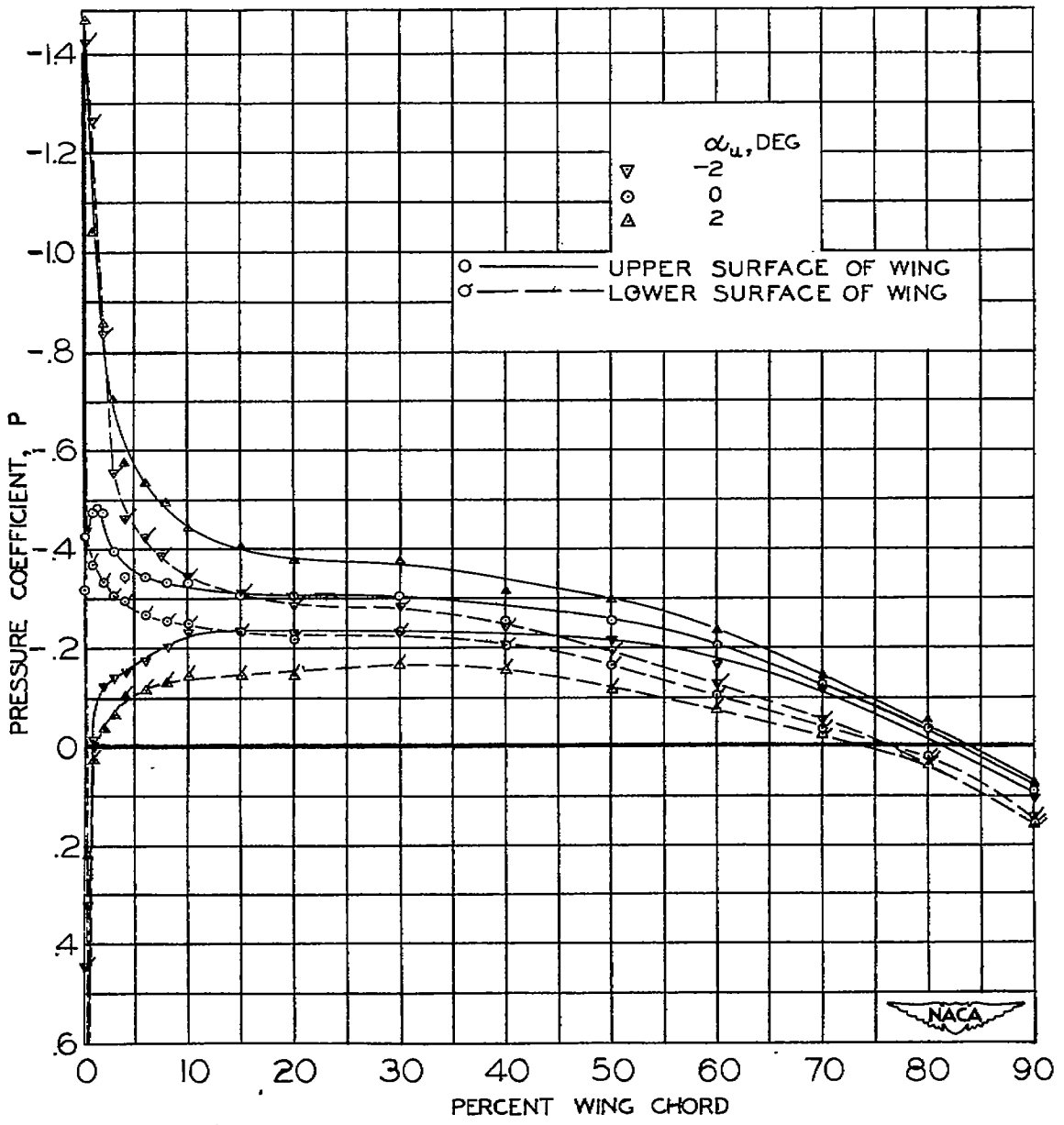

(a) INBOARD JUNCTURES

FIGURE 13.-PRESSURE DISTRIBUTION ALONG THE WING-NACELLE JUNCTURES FOR THE CENTRAL-FORWARD POSITION OF THE NACELLE.

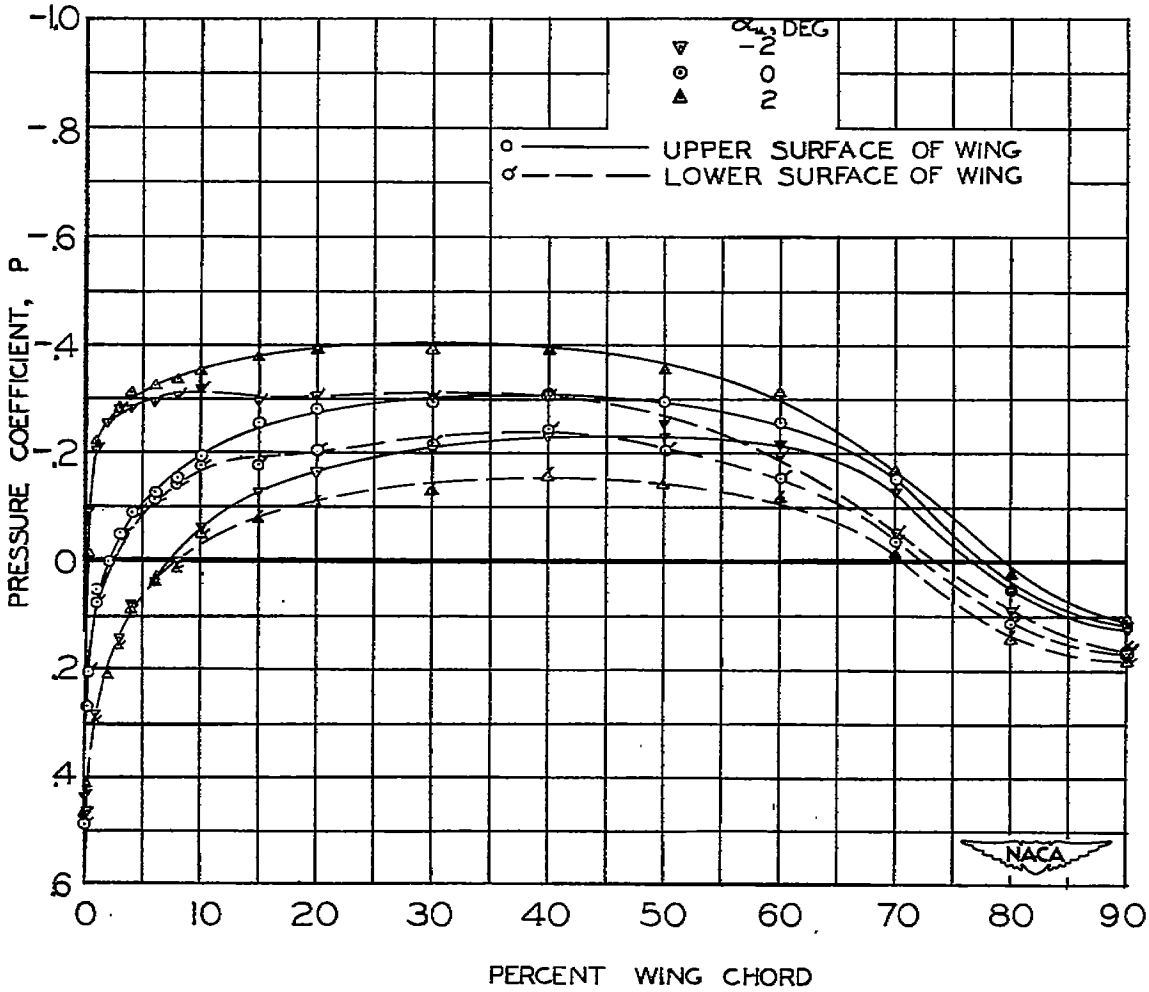

(b) OUTBOARD JUNCTURES

FIGURE 13. —CONCLUDED

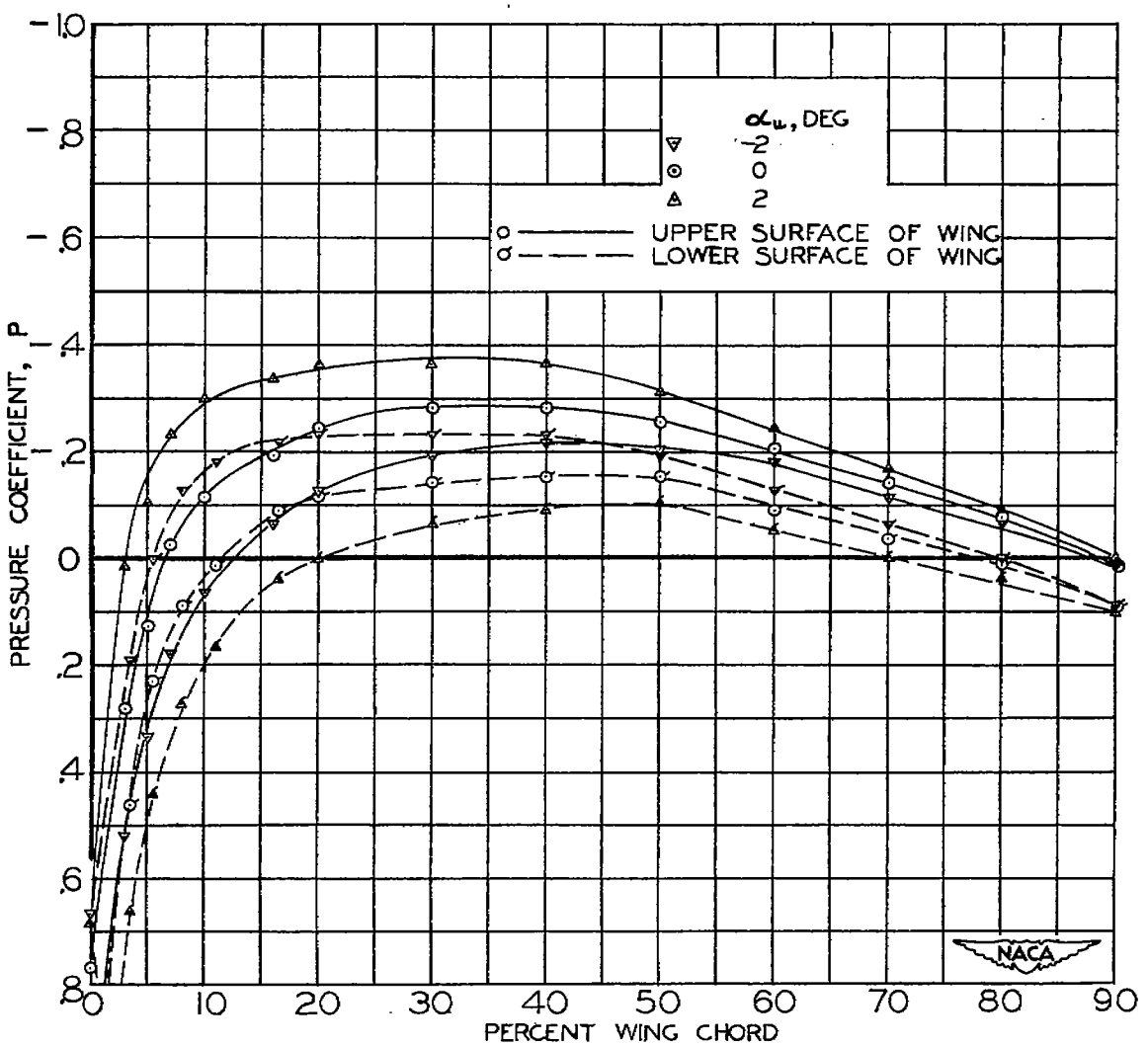

(a) INBOARD JUNCTURES

FIGURE 14.– PRESSURE DISTRIBUTION ALONG THE WING-NACELLE JUNCTURES FOR THE CENTRAL-COINCIDENT POSITION OF THE NACELLE.

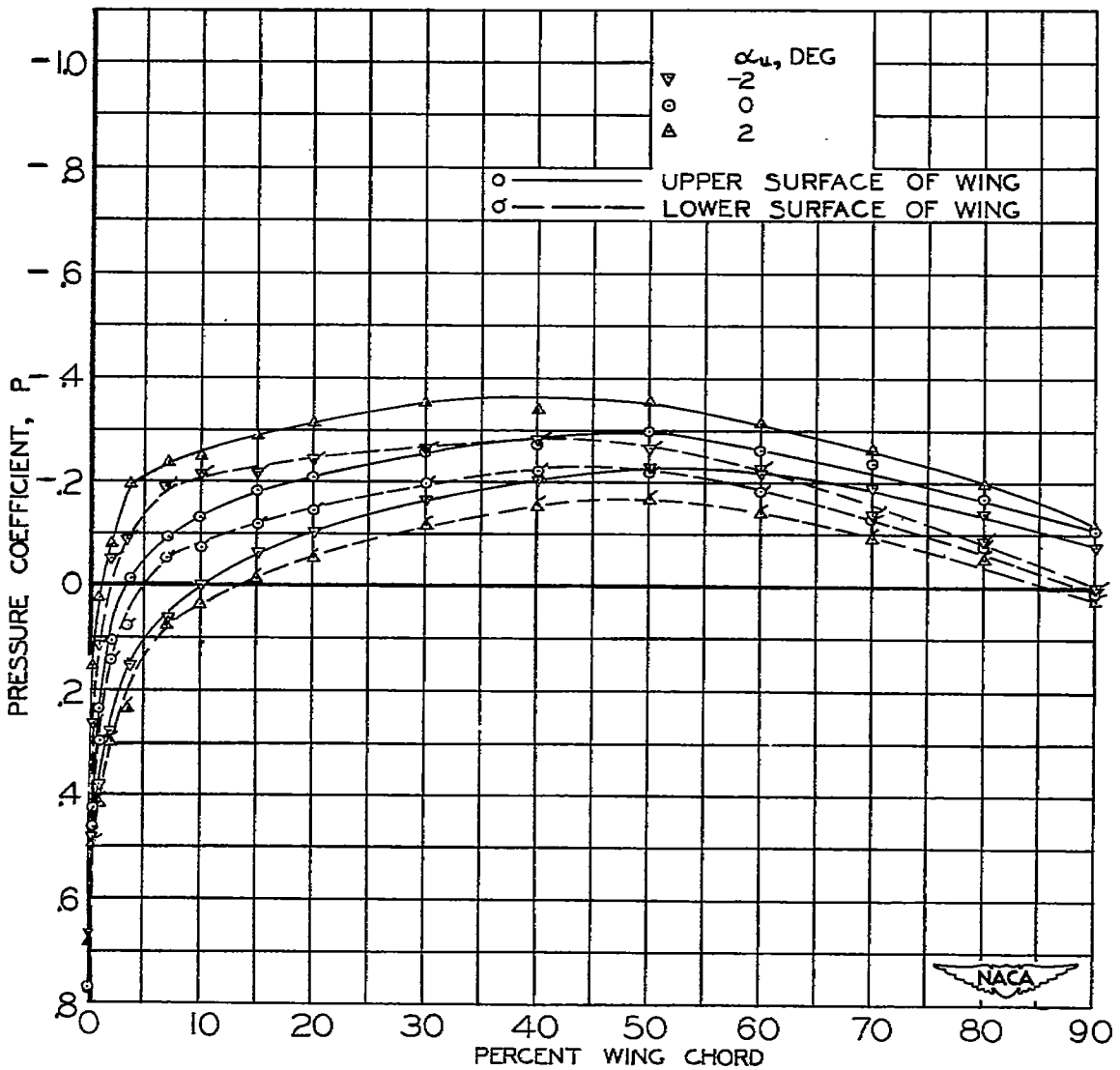

(b) OUTBOARD JUNCTURES

FIGURE 14.- CONCLUDED

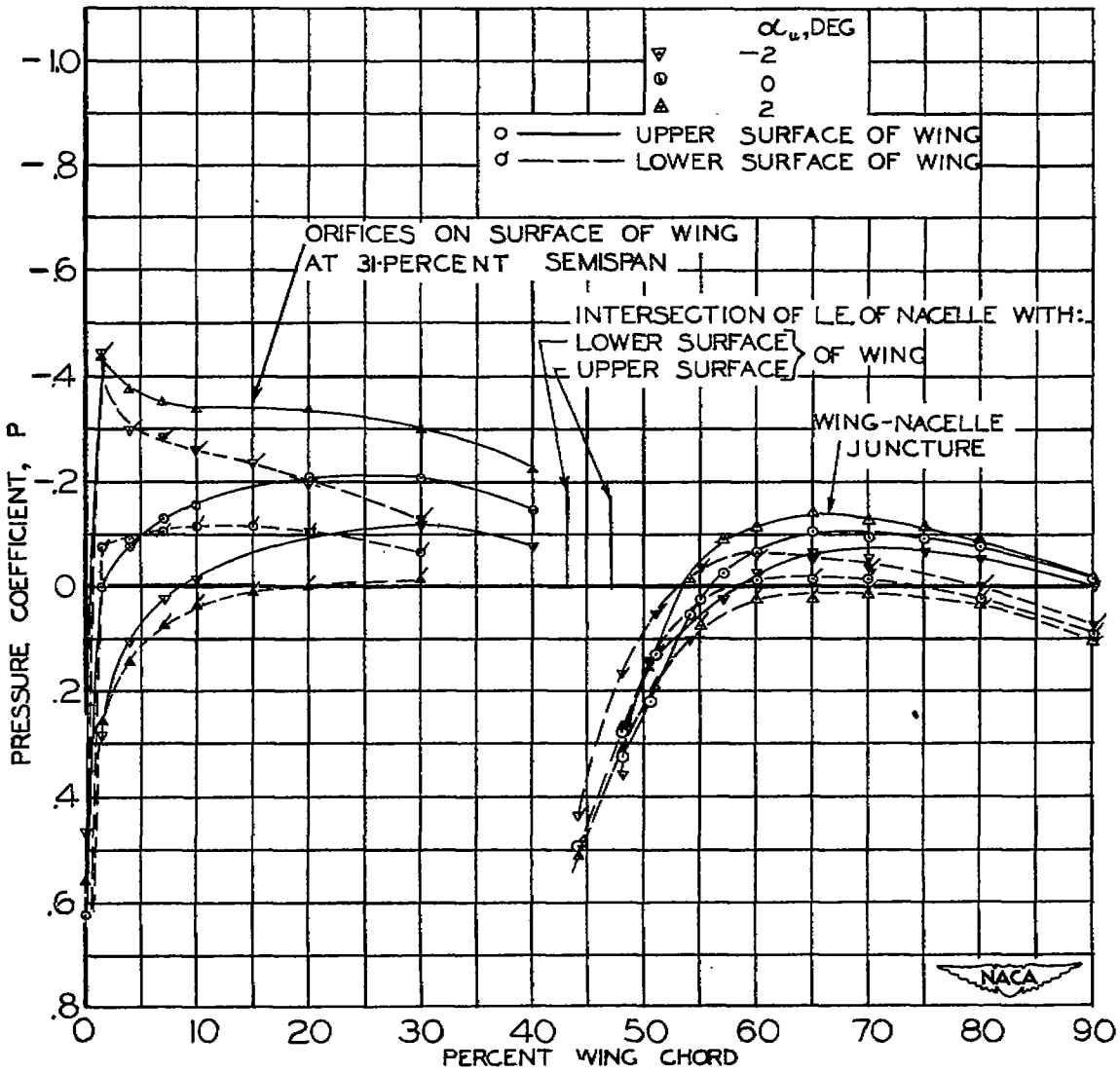

(a) INBOARD JUNCTURES

FIGURE 15.- PRESSURE DISTRIBUTION ALONG THE WING-NACELLE JUNCTURES FOR THE CENTRAL-AFT POSITION OF THE NACELLE.

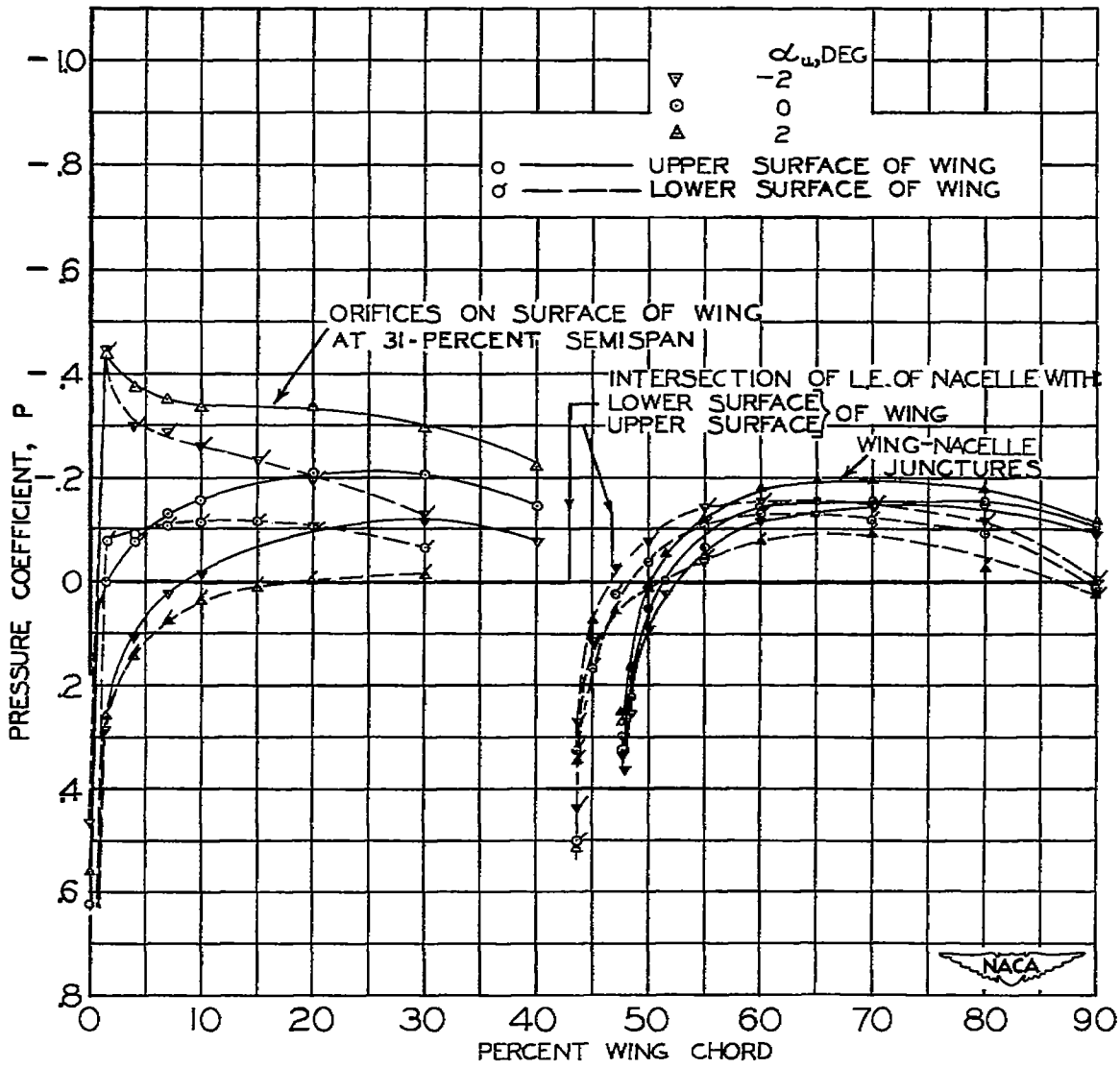

(b) OUTBOARD JUNCTURES

FIGURE 15. - CONCLUDED

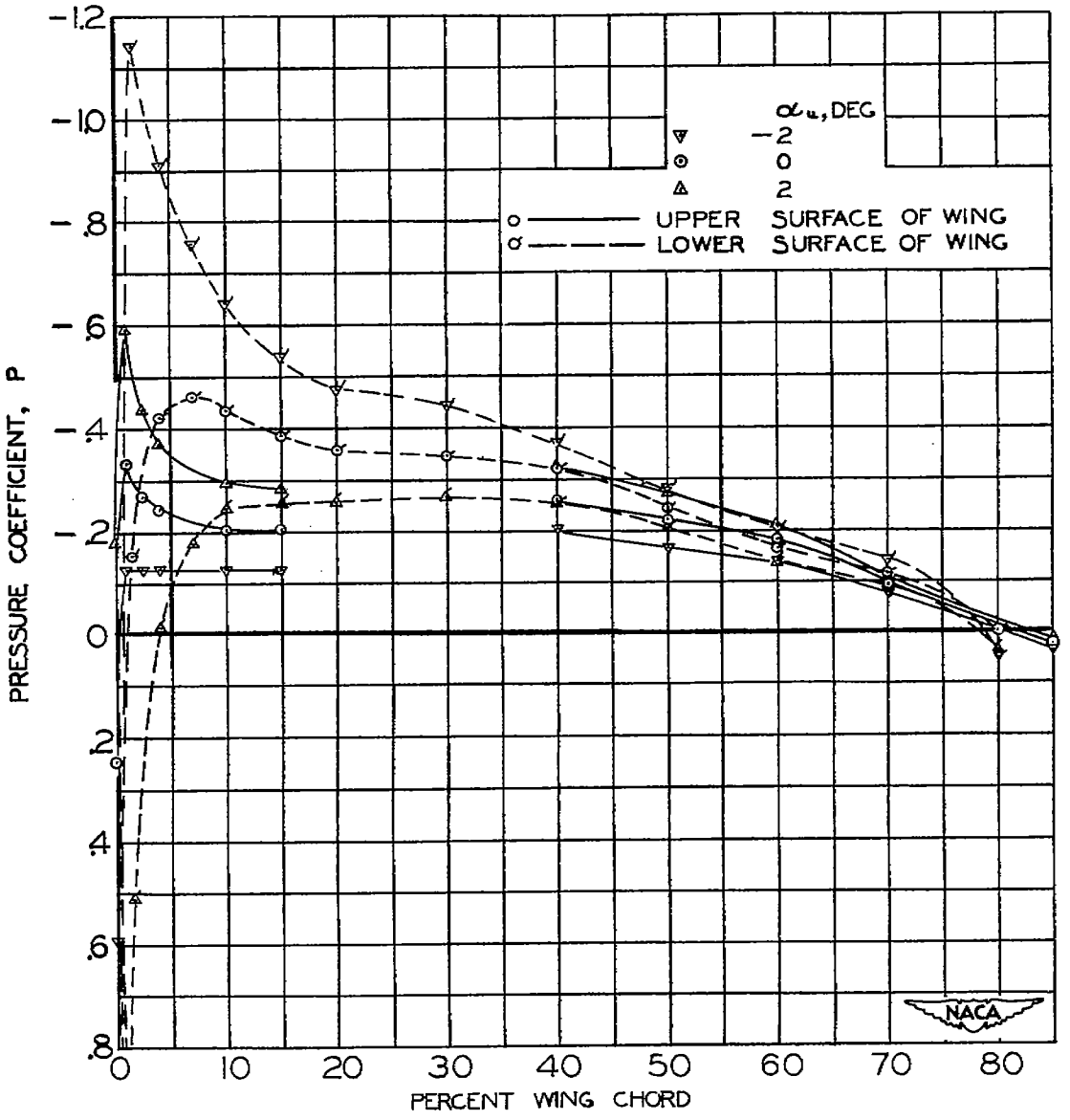

(a) INBOARD JUNCTURE

FIGURE 16.- PRESSURE DISTRIBUTION ALONG THE WING-NACELLE JUNCTURES FOR THE UNDERSLUNG-FORWARD POSITION OF THE NACELLE.

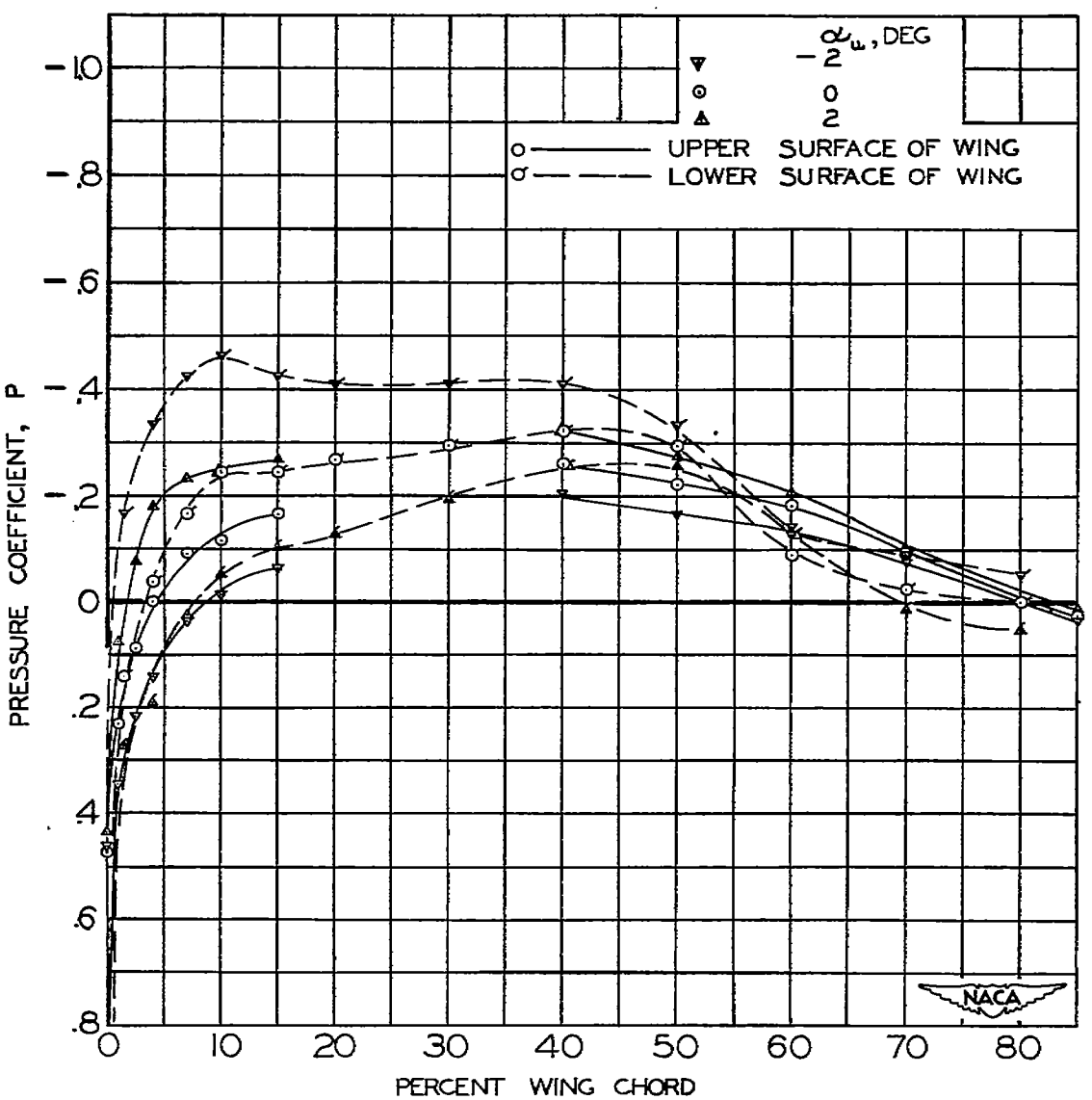

(b) OUTBOARD JUNCTURES

FIGURE 16. - CONCLUDED

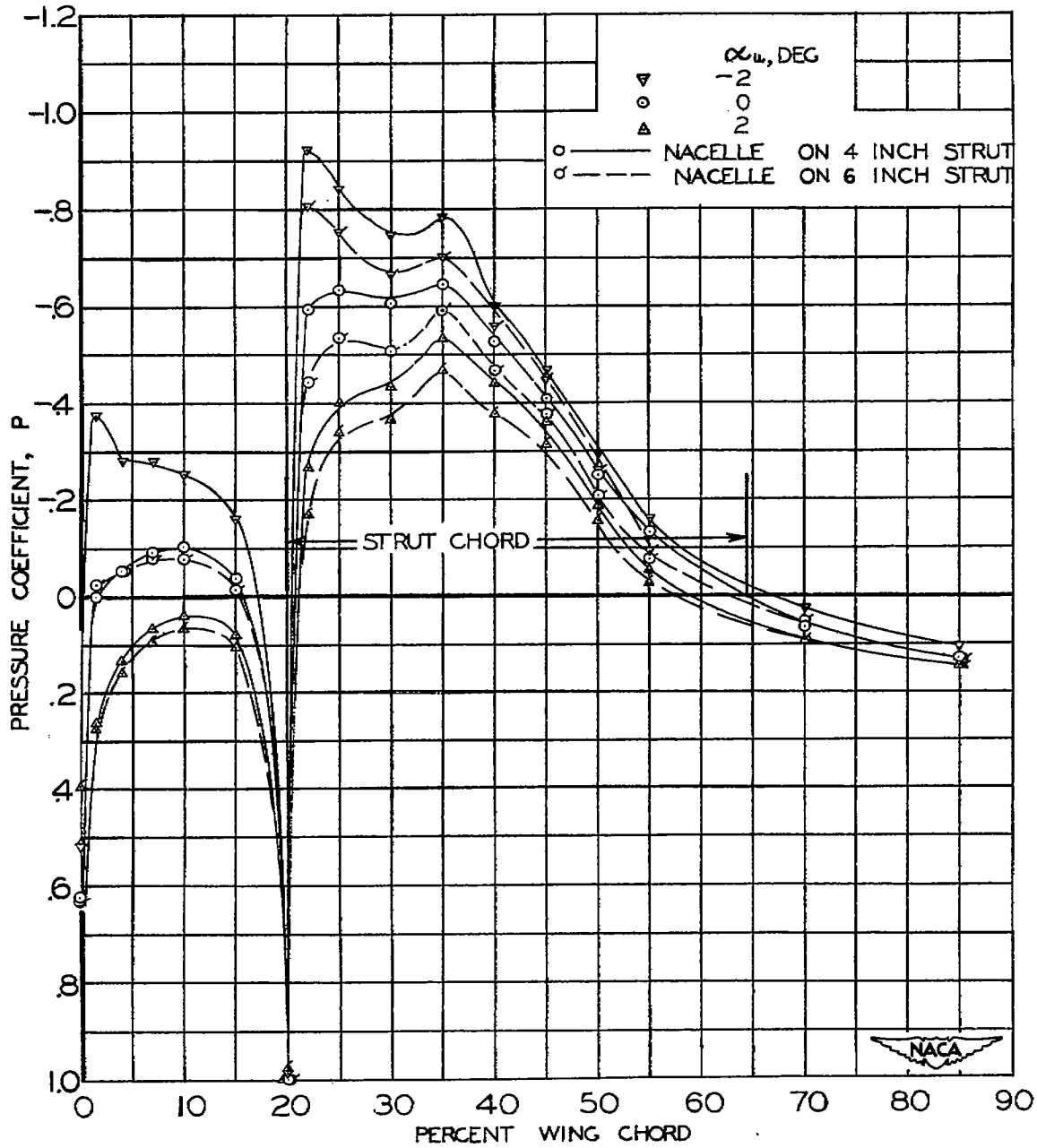

(a) INBOARD WING-STRUT JUNCTURE

FIGURE 17.– EFFECT OF STRUT LENGTH ON THE PRESSURE DISTRIBUTION IN THE WING-STRUT JUNCTURE FOR THE UNDERSLUNG-FORWARD POSITION OF THE NACELLE ON THE STRUT.

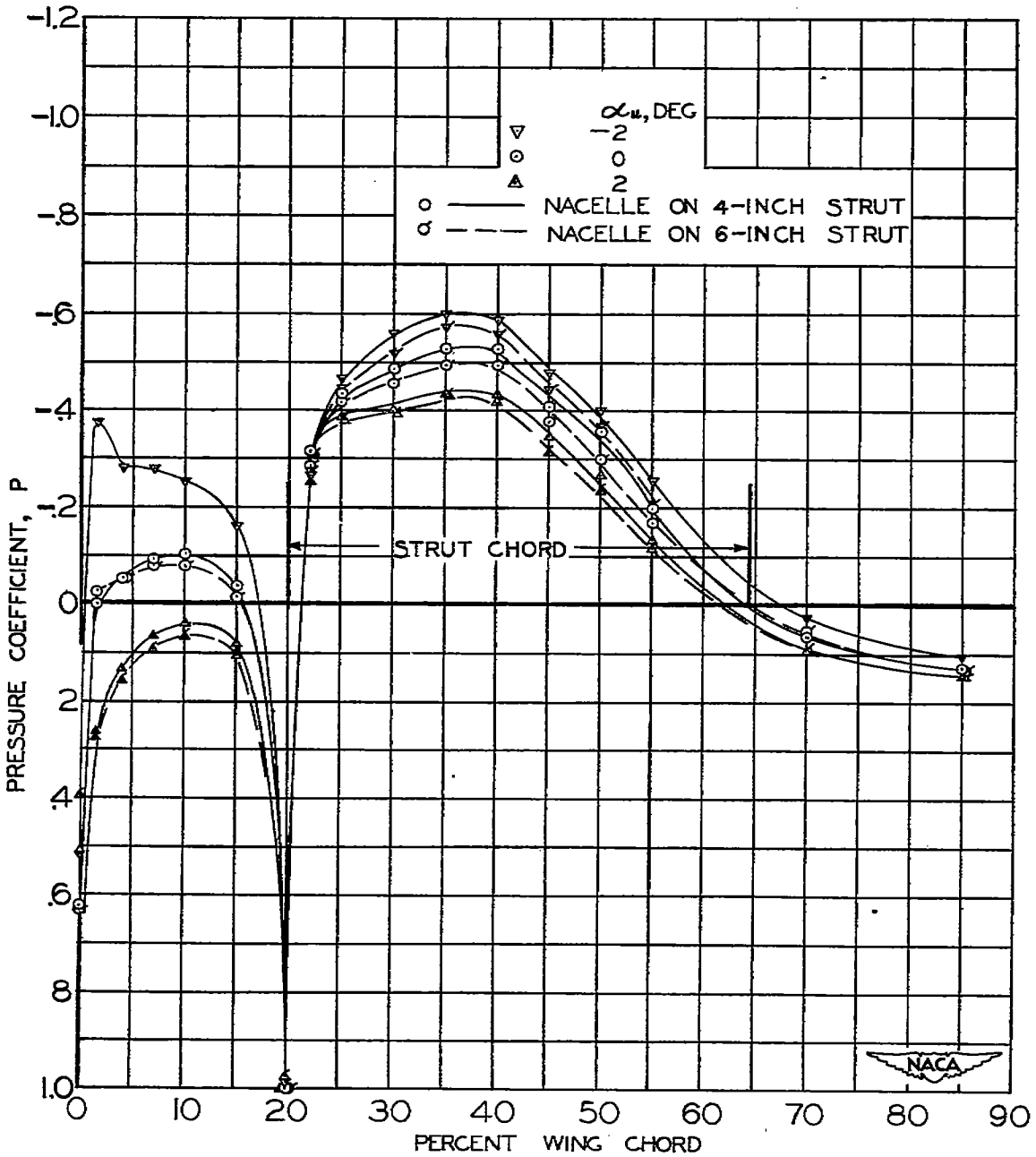

(b) OUTBOARD WING—STRUT JUNCTURE

FIGURE 17. – CONCLUDED

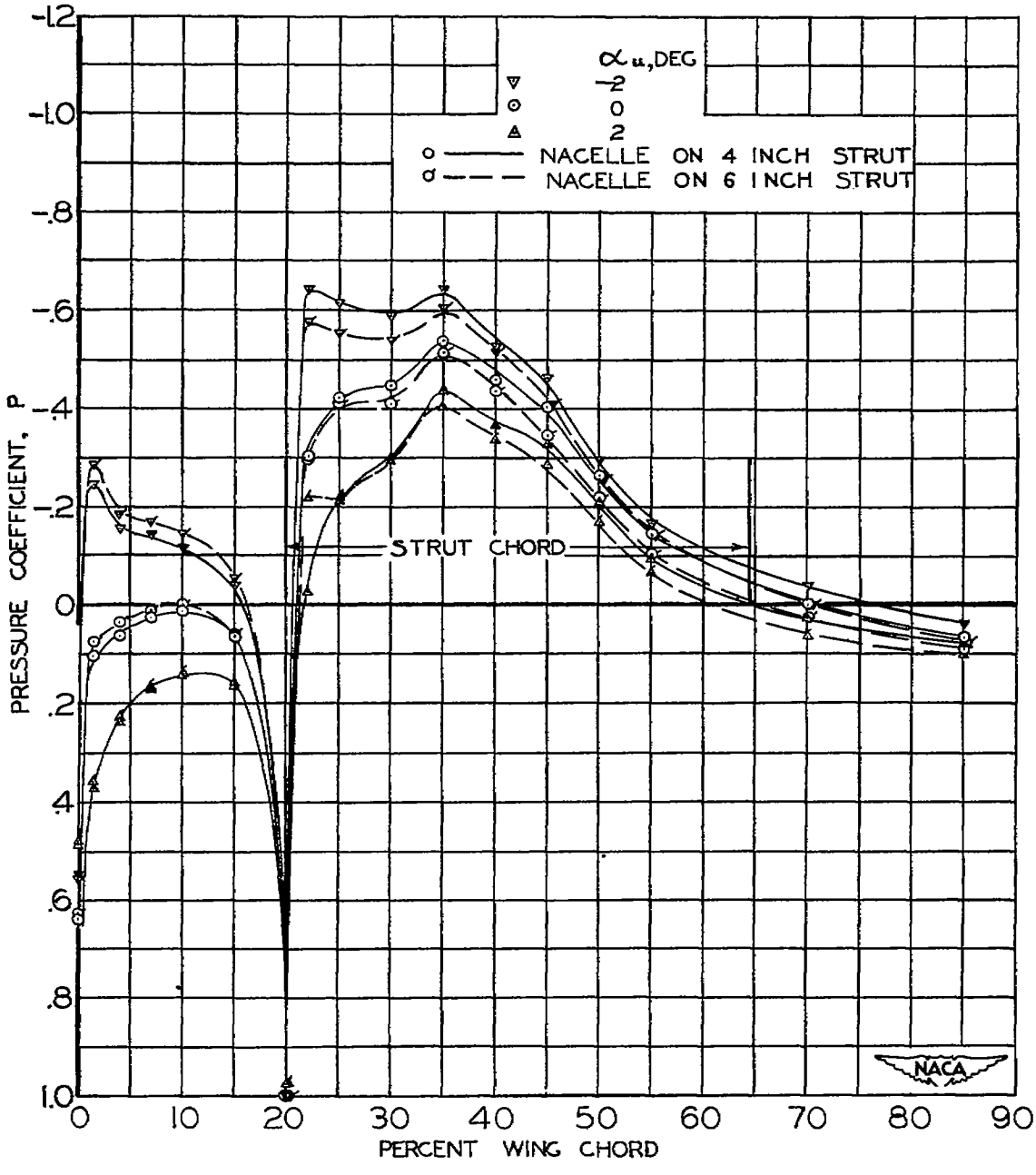

(a) INBOARD WING-STRUT JUNCTURE

FIGURE 18.- EFFECT OF STRUT LENGTH ON THE PRESSURE DISTRIBUTION IN THE WING-STRUT JUNCTURE FOR THE UNDERSLUNG-COINCIDENT POSITION OF THE NACELLE ON THE STRUT.

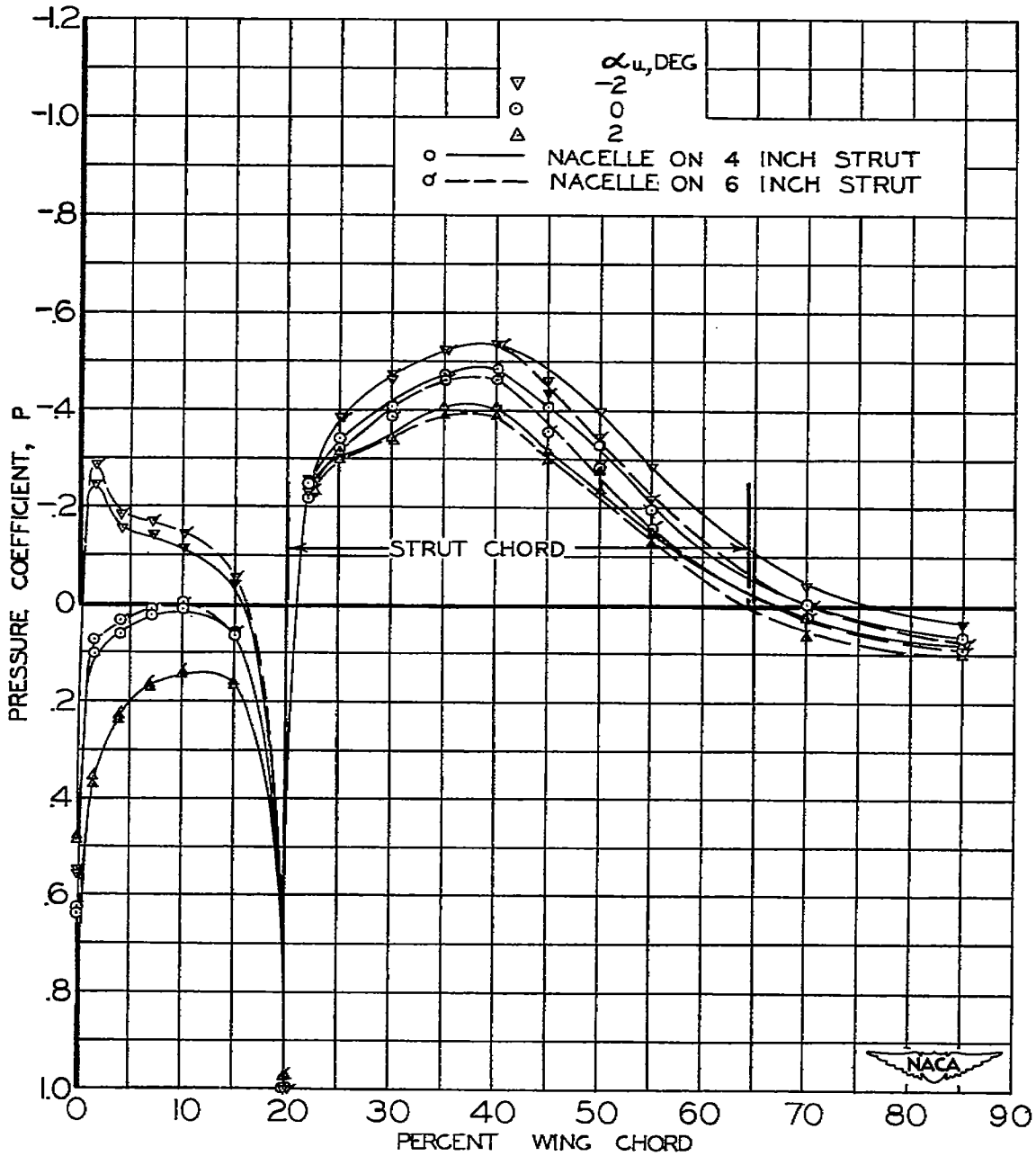

(b) OUTBOARD WING-STRUT JUNCTURE

FIGURE 18.- CONCLUDED

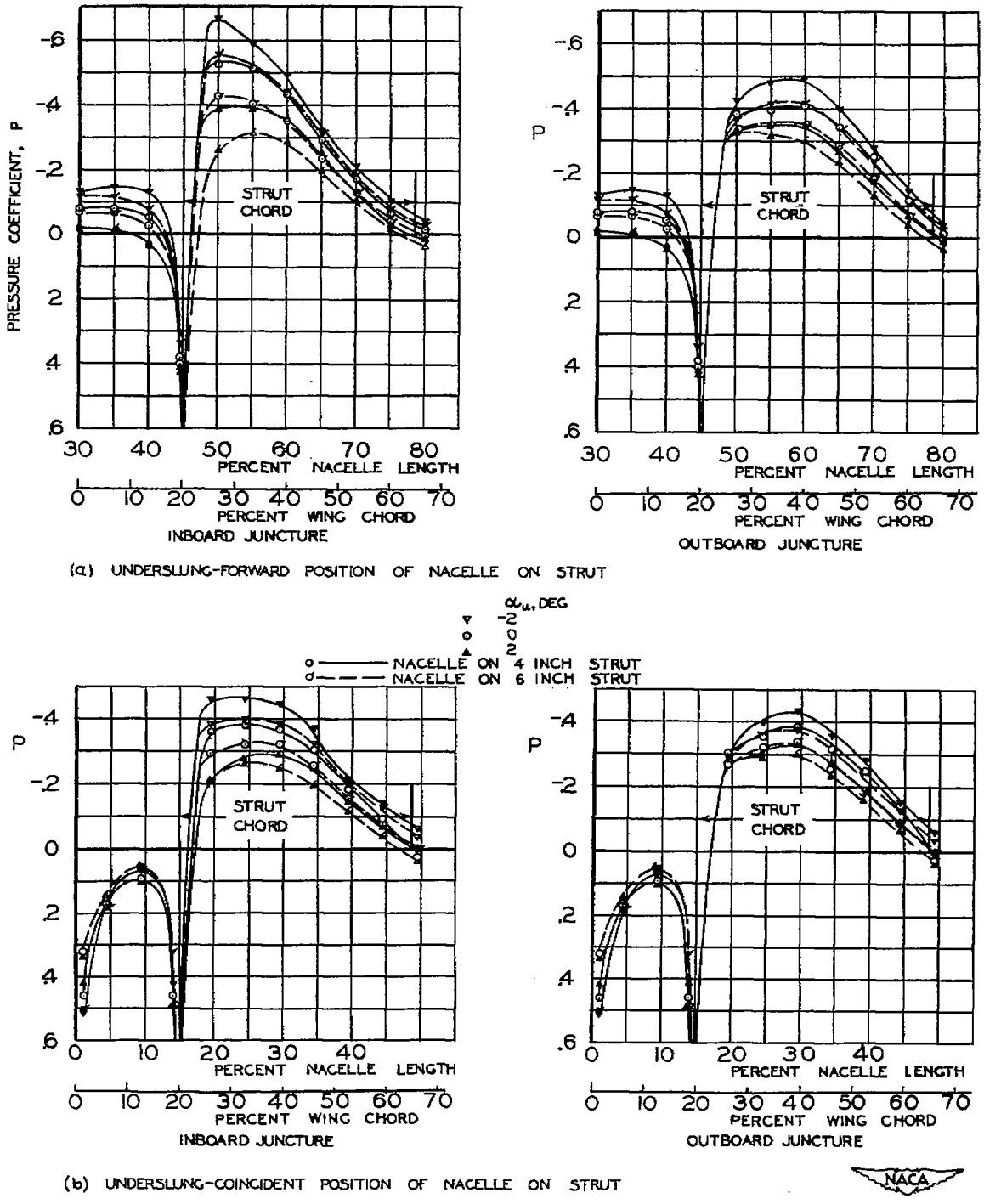

FIGURE 19.-EFFECT OF STRUT LENGTH ON THE PRESSURE DISTRIBUTION IN THE NACELLE JUNCTURES.

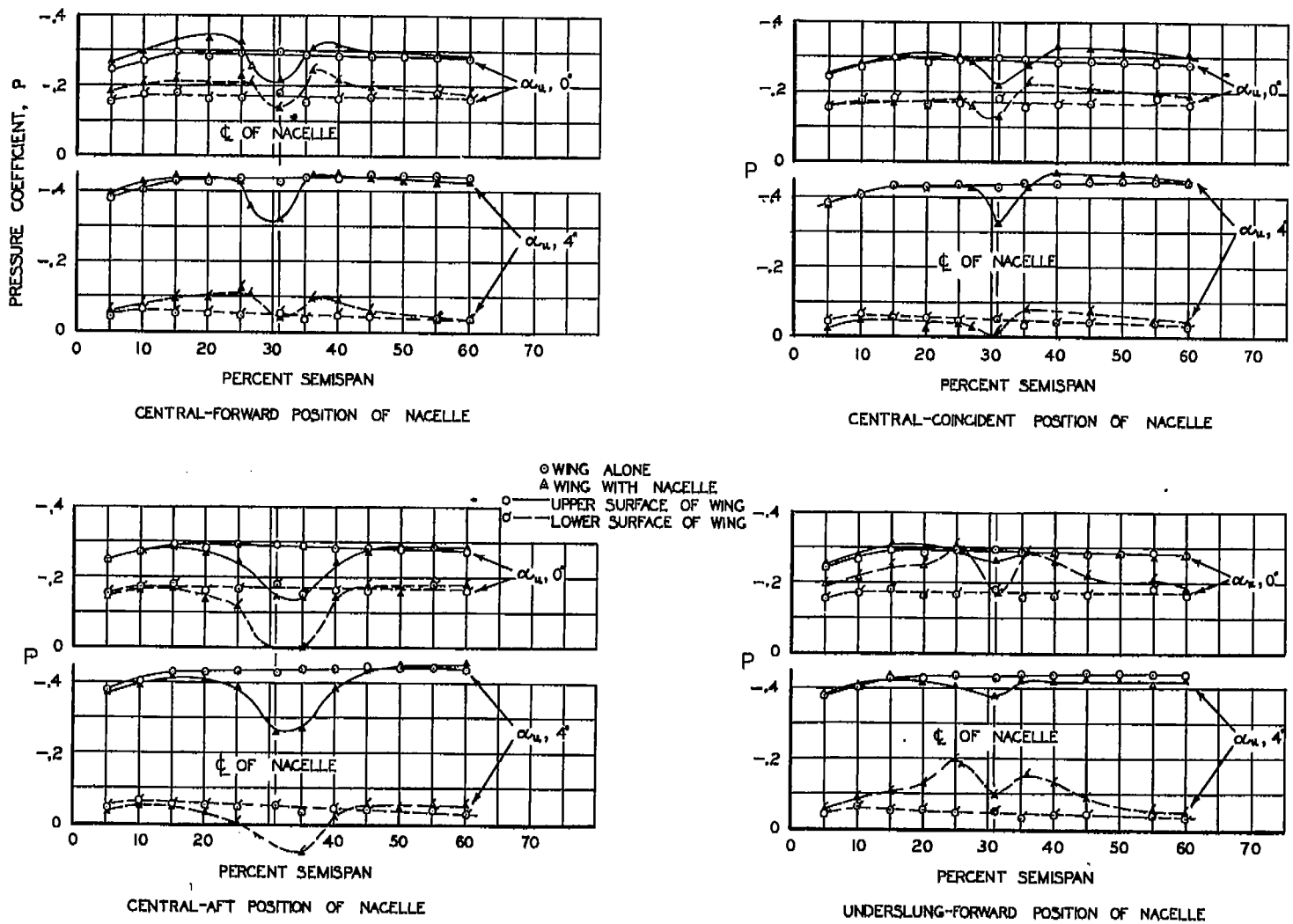

(a) NACELLE ON WING

FIGURE 20.-EFFECT OF THE NACELLE ON THE SPANWISE PRESSURE DISTRIBUTION AT 40-PERCENT WING CHORD.

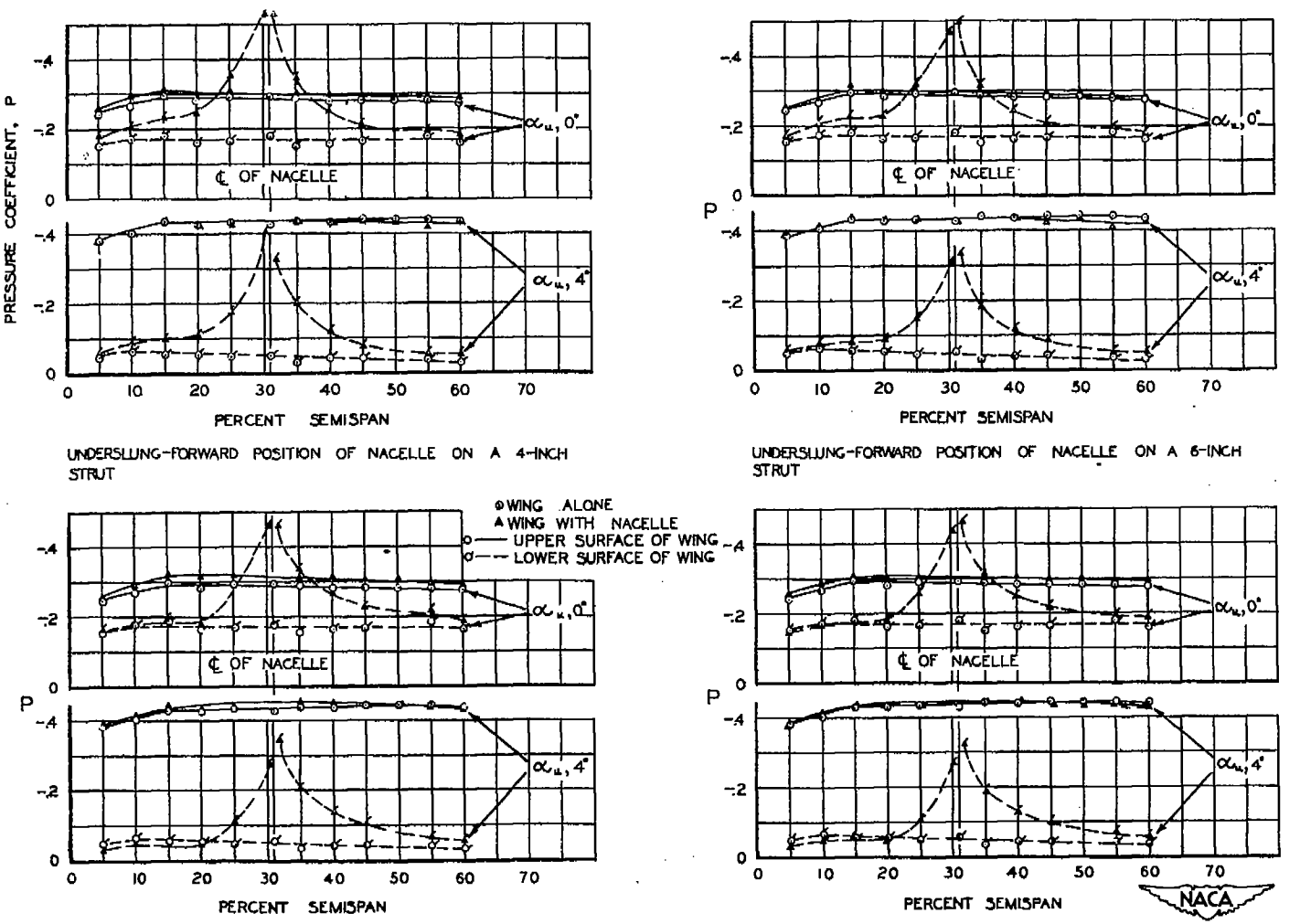

UNDERSLUNG-FORWARD POSITION OF NACELLE ON A 4-INCH STRUT

UNDERSLUNG-FORWARD POSITION OF NACELLE ON A 6-INCH STRUT

UNDERSLUNG-COINCIDENT POSITION OF NACELLE ON A 4-INCH STRUT

UNDERSLUNG-COINCIDENT POSITION OF NACELLE ON A 6-INCH STRUT

(b) NACELLE ON STRUT

FIGURE 20. - CONCLUDED

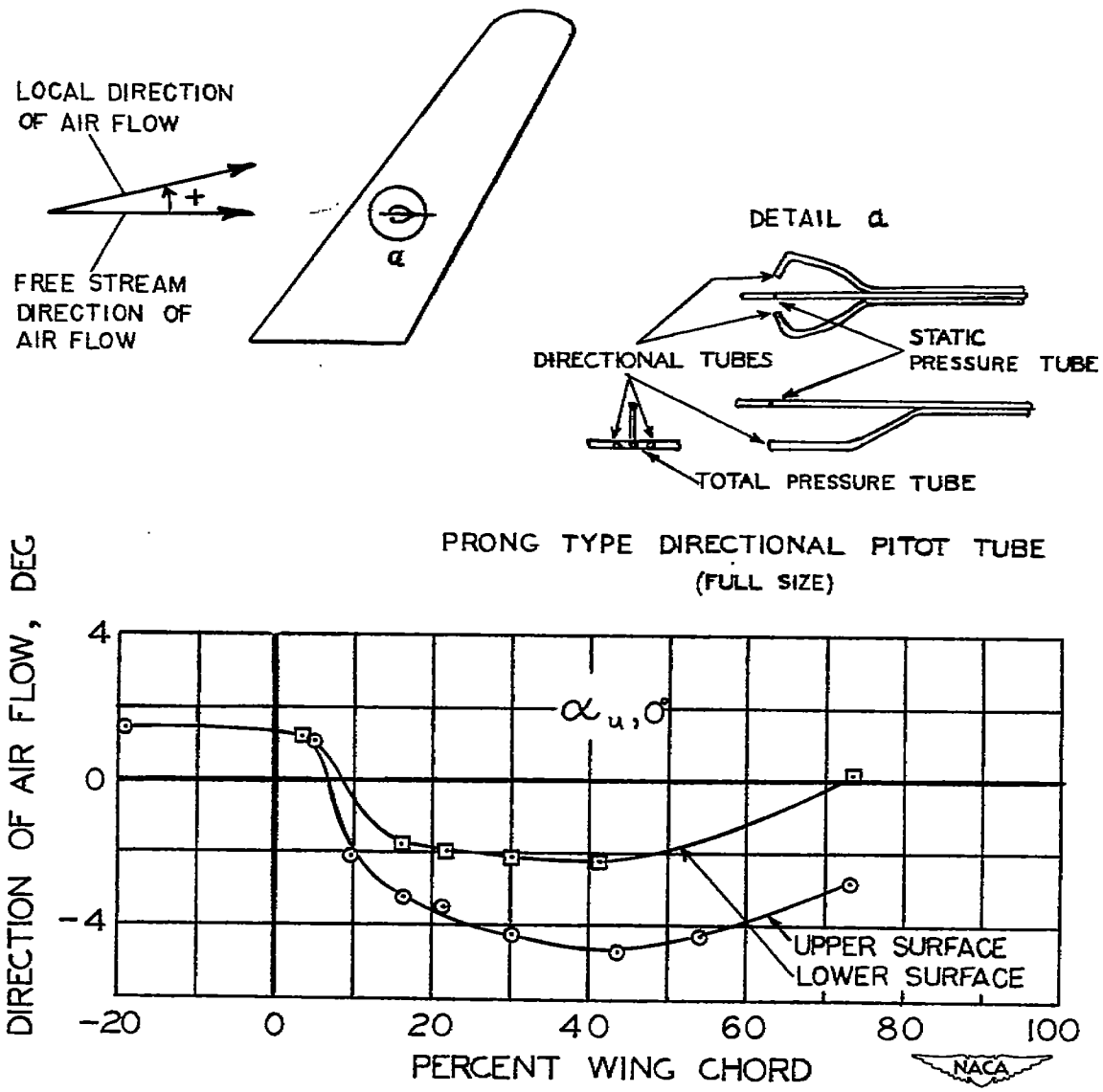

FIGURE 21.- DIRECTION OF AIR FLOW OVER THE SURFACE OF THE WING AT 31-PERCENT SEMISPAN.

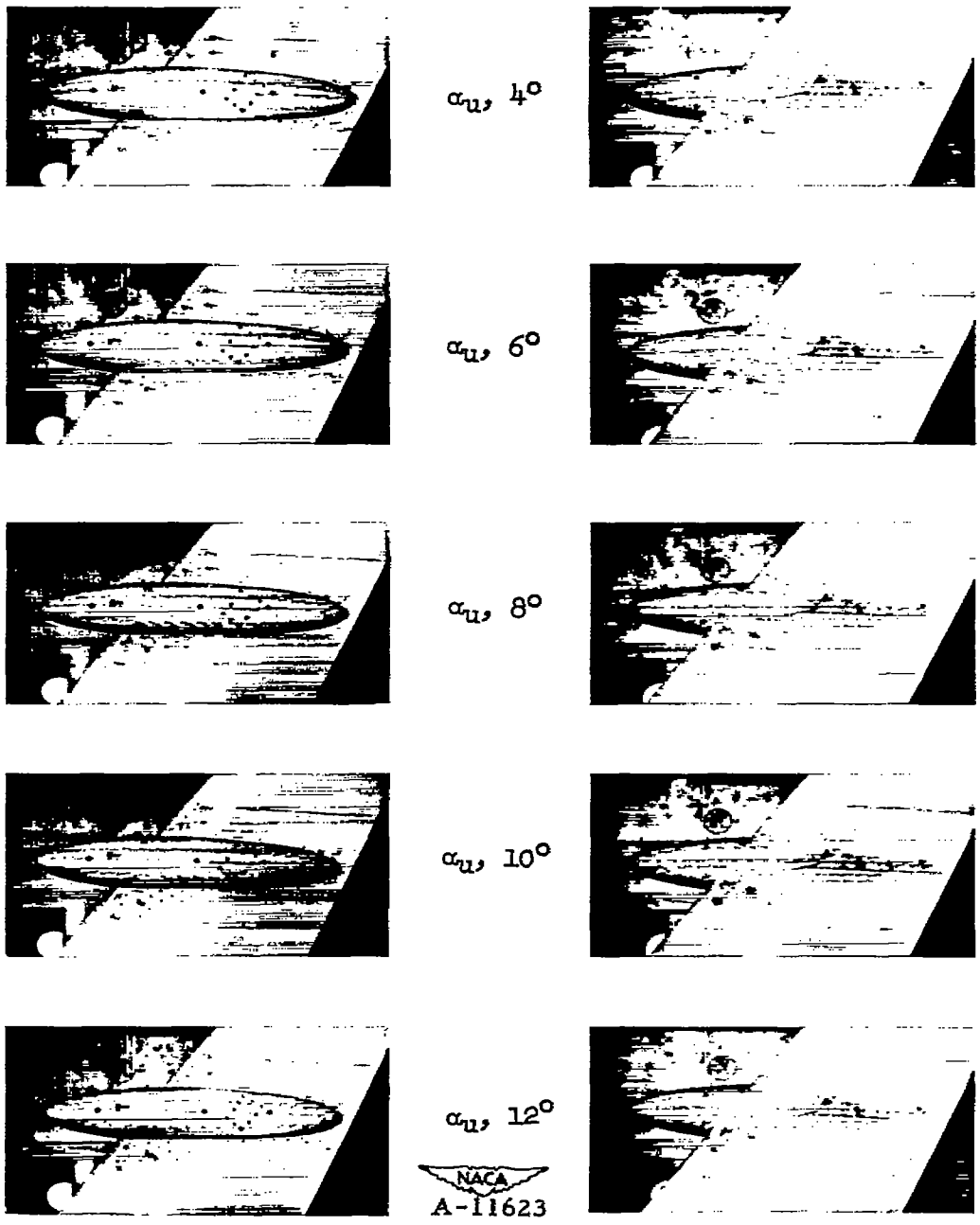

(a) Central-forward position of nacelle.

(b) Underslung-forward position of nacelle.

Figure 22.- Tuft studies over the upper surface of the wing and the nacelle.

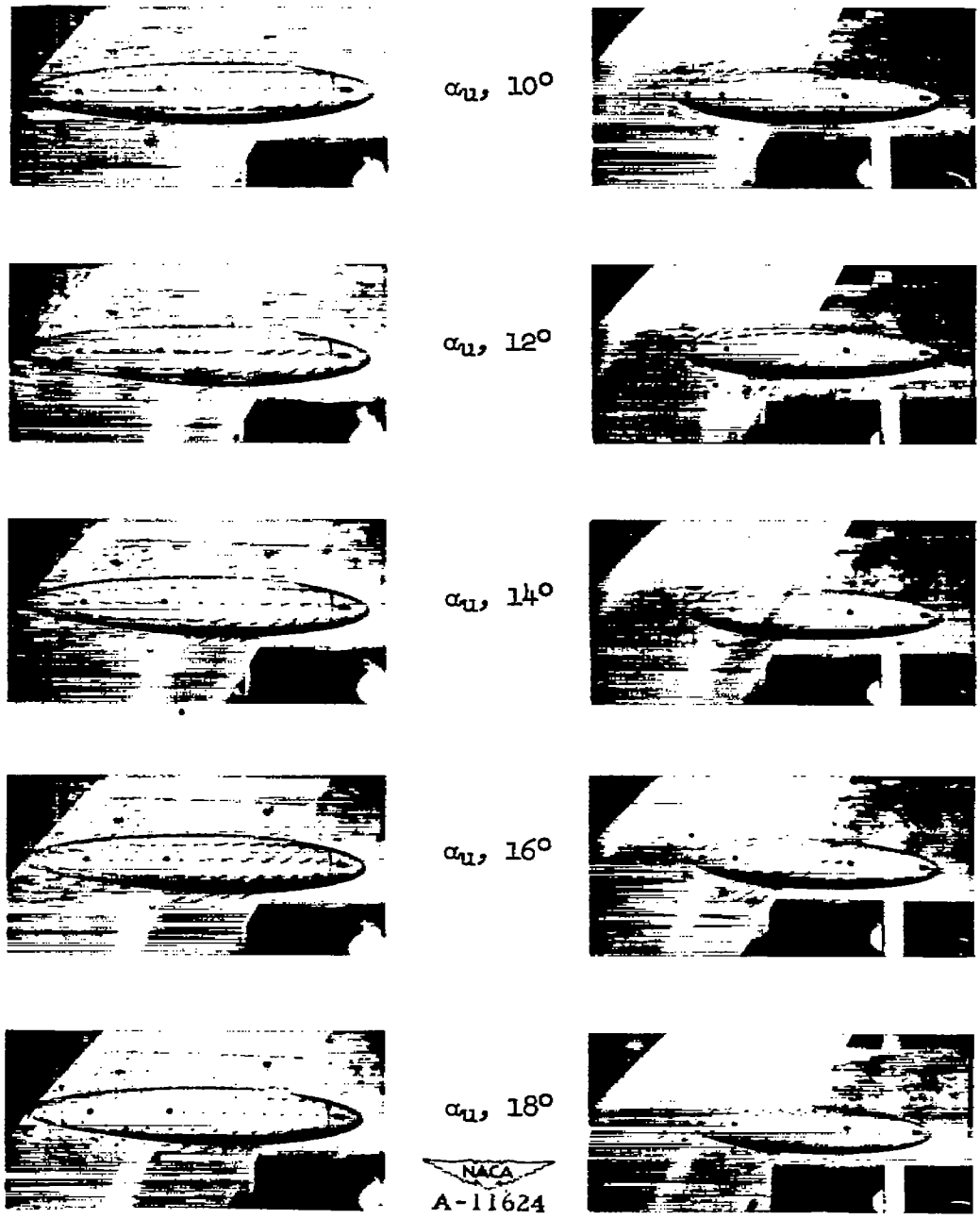

(c) Central-coincident position of nacelle.

(d) Central-aft position of nacelle.

Figure 22.- Concluded.

NASA Technical Library
3 1176 01434 4577